

## Surface Air Temperature and Precipitation Trends for Iceland in the 21st Century

---

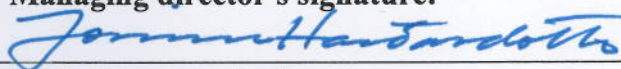
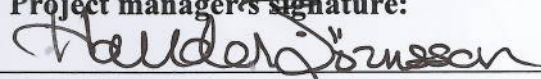
Nikolai Nawri  
Halldór Björnsson

# Surface Air Temperature and Precipitation Trends for Iceland in the 21st Century

---

Nikolai Nawri, Icelandic Meteorological Office  
Halldór Björnsson, Icelandic Meteorological Office

Keypage

<b>Report no.:</b> VÍ 2010-005	<b>Date.:</b> December 2010	<b>ISSN:</b> 1670-8261	<b>Public</b> <input checked="" type="checkbox"/> <b>Restricted</b> <input type="checkbox"/> <b>Provision:</b>
<b>Report title / including subtitle</b> Surface Air Temperature and Precipitation Trends for Iceland in the 21 <sup>st</sup> Century		<b>Number of copies:</b> 20	
		<b>Pages:</b> 42	
<b>Authors:</b> Nikolai Nawri and Halldór Björnsson		<b>Managing director</b> Jórunn Harðardóttir	
		<b>Project manager:</b> Halldór Björnsson	
<b>Project phase:</b>		<b>Project number:</b> 5811-0-0003	
<b>Report contracted for:</b> Climate and Energy Systems			
<b>Prepared in cooperation with:</b>			
<b>Summary:</b> In this study, the surface air temperature (SAT) and total precipitation (TP) trends over Iceland and the surrounding ocean area are determined, based on a reduced IPCC ensemble of General Circulation Model (GCM) simulations, as well as three Regional Climate Models (RCMs). It is found that SAT is likely to increase at a rate between 0.2–0.4 K per decade until 2050 over land with superimposed decadal variations determined by natural climate variability, and a somewhat smaller trend of 0.15–0.30 K per decade over the ocean. If, as assumed in the A1B scenario, global population and CO <sub>2</sub> emissions decrease after 2050, the reduced IPCC ensemble used in this study predicts that SAT will increase at a reduced rate of about 0.2 K per decade in the second half of the 21 <sup>st</sup> Century. With TP, inter-annual fluctuations and inter-model differences are significantly larger than for SAT. However, based on the reduced IPCC ensemble, it is likely that TP will increase at a rate of about 1% of the 1961–90 average per decade throughout the 21 <sup>st</sup> Century, with somewhat lower trends over the ocean than over land areas.			
<b>Keywords:</b> Climate change, climate scenarios, Iceland, dynamic down-scaling		<b>Managing director's signature:</b> 	
		<b>Project manager's signature:</b> 	
		<b>Reviewed by:</b> ToJ, SG	



# Contents

<b>1</b>	<b>Introduction</b>	<b>9</b>
<b>2</b>	<b>Data and Methodology</b>	<b>11</b>
<b>3</b>	<b>Spatial Variability of Climate Trends</b>	<b>13</b>
3.1	Surface Air Temperature . . . . .	13
3.2	Total Precipitation . . . . .	15
<b>4</b>	<b>Long-Term Trends of Annual Mean Values</b>	<b>16</b>
4.1	Surface Air Temperature . . . . .	17
4.2	Total Precipitation . . . . .	19
<b>5</b>	<b>Seasonal Differences in Climate Trends</b>	<b>20</b>
<b>6</b>	<b>Conclusions</b>	<b>21</b>

# List of Figures

1	Mean annual surface air temperature during the 1961–90 control period, differences in degrees between the control period and the 2021–50 reference period, and linear trends in degrees per decade within the 2004–50 period, for the IPCC GCM ensemble mean, the SMHI-RCAO, the MetNo-HIRHAM, and the DMI-HIRHAM5.	23
2	Mean annual surface air temperature and total precipitation during the 1961–90 control period.	24
3	Dependence on terrain elevation of surface air temperature and total precipitation in the RCMs during the 1961–90 control period in winter (DJF) and summer (JJA).	25
4	Differences between summer (JJA) and winter (DJF) mean seasonal surface air temperature in degrees centigrade during the 1961–90 control period, for the reanalyses and the RCMs.	26
5	Dependence on terrain elevation of linear trends of surface air temperature within the 2004–50 period in the SMHI-RCAO, the MetNo-HIRHAM, and the DMI-HIRHAM5, together with the corresponding model orographies.	27
6	Mean annual surface air temperature in degrees centigrade during the 1961–90 control period, differences in degrees between the control period and the 2021–50 reference period, and linear trends in degrees per decade within the 2004–50 period, for the UKMO HadCM3, and the MPI ECHAM5-r3.	28
7	Mean annual surface air temperature and total precipitation during the 1961–90 control period, and linear trends within the 1958–2001 period, for the ERA-40 reanalyses.	29
8	Differences between the RCM and underlying GCM simulations of mean annual surface air temperature: mean fields in degrees centigrade during the 1961–90 control period, differences in degrees between the control period and the 2021–50 reference period, and linear trends in degrees per decade within the 2004–50 period, for the SMHI-RCAO, the MetNo-HIRHAM, and the DMI-HIRHAM5.	30
9	Mean annual total precipitation in millimetres per day during the 1961–90 control period, differences in percent of the control period between the control period and the 2021–50 reference period, and linear trends in percent of the control period per decade within the 2004–50 period, for the IPCC GCM ensemble mean, the SMHI-RCAO, the MetNo-HIRHAM, and the DMI-HIRHAM5.	31
10	Mean annual air pressure at mean sea level in hectopascals during the 1961–90 control period, for the reanalyses and the RCMs.	32
11	Dependence on terrain elevation of linear trends of total precipitation within the 2004–50 period in the SMHI-RCAO, the MetNo-HIRHAM, and the DMI-HIRHAM5, together with the corresponding model orographies.	33

12	Mean annual total precipitation in millimetres per day during the 1961–90 control period, differences in percent of the control period between the control period and the 2021–50 reference period, and linear trends in percent of the control period per decade within the 2004–50 period, for the UKMO HadCM3, and the MPI ECHAM5-r3. . . . .	34
13	Differences between the RCM and underlying GCM simulations of mean annual total precipitation: mean fields in millimetres per day during the 1961–90 control period, differences in millimetres per day between the control period and the 2021–50 reference period, and linear trends in millimetres per day per decade within the 2004–50 period, for the SMHI-RCAO, the MetNo-HIRHAM, and the DMI-HIRHAM5. . . . .	35
14	Mean annual values of surface air temperature and total precipitation, averaged over the land area of Iceland, for the reanalyses, the GCM ensemble mean, and the RCMs. . . . .	36
15	Mean annual values of surface air temperature over Iceland based on 24 RCMs included in the ENSEMBLES project. . . . .	37
16	Mean seasonal cycle during the 1961–90 control period, the 2021–50 reference period, and the 2070–99 reference period, for the IPCC ensemble mean, the SMHI-RCAO, the MetNo-HIRHAM, and the DMI-HIRHAM5. . . . .	38
17	Changes in the mean seasonal cycle from the 1961–90 control to the 2021–50 reference period, as well as changes from the control to the 2070–99 reference period, for the reduced IPCC ensemble mean, the SMHI-RCAO, the MetNo-HIRHAM, and the DMI-HIRHAM5. . . . .	39
18	Warming by month from the 1991–2000 to the 2091–2100 period in ENSEMBLES RCMs using either the HadCM3 or the ECHAM5 as driving GCM. . . . .	40





# 1 Introduction

Future projections of regional climate are of great importance for policy makers and adaptation planning. However, compared with global climate simulations, predictions of regional climate are complicated by the consideration of a more complex geography (such as topography and land-surface classes), and by the necessity of representing more detailed physical processes occurring over shorter periods of time and over smaller spatial scales.

In general, regional climate projections are derived either directly from one or more general circulation model (GCM) runs, or through additional numerical or statistical downscaling of these large-scale fields. Numerical downscaling uses higher-resolution regional climate models (RCMs) over a limited area to refine global GCM simulations. Problems arise if the necessary detailed geographical information is not available on a suitable scale. Furthermore, changes in geographical conditions (such as the retreat of glaciers, or a change in sea ice cover and vegetation) may affect the local climate, making it necessary to include the representation of local feedback mechanisms between the atmosphere and other components of the ecosystem. The representation of these factors is still lacking or at best rudimentary in most RCMs. While adding more detail to regional climate studies, numerical downscaling is sensitive to various errors and biases in the GCM dynamics that may average out globally, but are present on the regional scale. In an attempt to minimise GCM errors, statistical downscaling methods correct GCM projections based on local weather data (Engen-Skaugen, 2007). Thereby, however, it is assumed that certain statistical relationships between observed climate conditions and GCM control runs remain valid as climatic conditions change, which may not be justified.

The earliest published future climate scenarios for Iceland based on GCM results appeared in Bergþórsson et al. (1987), using results from equilibrium experiments with the GISS climate model (Hansen et al., 1983, 1984). Differences between the  $1\times\text{CO}_2$  and  $2\times\text{CO}_2$  equilibrium experiments were used to estimate greenhouse effects. Interpolated to Stykkishólmur, the warming annually was about  $4^\circ\text{C}$ , but ranging over the course of the year between  $4.1\text{--}4.3^\circ\text{C}$  from November to April, and between  $3.6\text{--}3.8^\circ\text{C}$  from June to September. Thus the wintertime warming exceeded that during the summer by about half a degree. Adding the calculated warming for the  $2\times\text{CO}_2$  equilibrium to the observations at Stykkishólmur, resulted in predicted temperatures close to those at Bergen, Norway during the summer, and to those at Lerwick, Shetland Islands during the winter. The study also examined projected changes in precipitation and found that on an annual basis precipitation increased from 704 mm to 809 mm, or by about 15%, without significant seasonal differences. While this study gave insight into how Icelandic climate might change in response to increasing  $\text{CO}_2$  levels, it did not address how various climate variables might change specifically over the course of the 21<sup>st</sup> Century.

For Iceland, this was first done by Jóhannesson et al. (1995), who used statistical downscaling results previously obtained by Kaas (1993, 1994), as well as results from four different climate models (with the GFDL CM3 as the primary reference). The study found a warming of 0.3 K per decade until the middle of the 21<sup>st</sup> Century, with a wintertime warming rate of 0.35 K per decade, and a warming rate of 0.25 K per decade in summer. The study also examined precipitation changes and found a 1.50% per decade increase in precipitation on an annual basis, with a higher rate of increase during the winter (1.75% per decade) than in summer (1.25% per decade). These

estimates, together with bounds based on past natural variability, were used for the reports by the Icelandic Science Committee on Climate Change (Ministry for the Environment, 2000, 2008).

The next published study focusing on climate projections for Iceland was by Jónasson (2004), who used an auto-regressive model of past climate variability to determine forced warming trends. The assumed underlying warming trend was based on a literature review of GCM studies and amounted to 0.23 K per decade until 2020 and 0.28 K per decade after that. The innovative part of this study was in estimating the probability distribution of warming at 5 year intervals during the 21<sup>st</sup> Century. For the mid-21<sup>st</sup> Century, the 90% confidence interval for warming relative to the 1961–90 average in Reykjavik of 4.3°C is 0.6–3.3 K, and 1.4–5.9 K at the end of the century.

As part of the Climate and Energy (CE) project (Fenger, 2007), and its Icelandic counterpart, the Veður og Orka (VO) project, various climate change predictions for Iceland were made. The CE project used an ensemble of six GCMs and RCMs from the PRUDENCE project for four different emissions scenarios (B1, B2, A2, and A1FI) developed by the Intergovernmental Panel on Climate Change (IPCC). The GCMs used by the CE project showed more warming during winter than summer. During winter, the median projected warming from 1961–90 to 2070–99 ranged from 3–6 K, and from 2–3 K during summer (corresponding approximately to 0.3–0.6 K per decade during winter, and 0.2–0.3 K per decade during summer). The amount of warming was greater for the high than for the low emissions scenarios, as was the model spread. Furthermore, there was greater model spread and internal model variability in the wintertime results compared with those for summer. For the highest emitting scenario, precipitation increased by 10–15% from 1961–90 to 2070–99, and by 5–10% for the lower emitting scenarios (corresponding to approximately 0.5–1% per decade).

The CE project also examined RCM results for Iceland based on the HIRHAM model (Haugen and Iversen, 2006). These results showed enhanced warming over the interior of Iceland compared with the coastal zone, and a tendency for enhanced warming towards the northeast. The warming from 1961–90 to 2070–99 on an annual basis was about 1 K in the southwest of Iceland, but reached 2–3 K in the interior and on the east coast. Of the two emission scenarios used (A2 and B2), the higher emitting one (A2) produced slightly more warming, but a very similar spatial structure. The HIRHAM results also showed an increase in precipitation, with more increase in coastal areas in the north and east of Iceland, but with less increase over the interior.

The HIRHAM results were examined in more detail in the VO project (Jóhannesson et al., 2007). The two scenarios of the HIRHAM runs were averaged to yield one reference scenario. The spatial average of the reference scenarios for the country as a whole yielded annual average warming of 2.8 K from 1961–90 to 2070–99 (or 0.25 K per decade), and the corresponding precipitation increase was 6% (or 0.55% per decade). The change in the seasonal cycle in the HIRHAM results deviated from the results found by earlier GCM studies. As described above, previous GCM studies tended to produce more warming during winter than summer, with spring and autumn warming rates falling in between. However, in the HIRHAM results, warming was largest during autumn, followed by spring, summer, and winter. Seasonal differences in precipitation change were such that the largest increase occurred during autumn.

Finally, as part of the 2008 report by the Icelandic Science Committee on Climate Change (Ministry for the Environment, 2008), climate change predictions for Iceland based on GCM models

from the CMIP-3 dataset were generated. Three emissions scenarios (B1, A1B, and A2) were examined for the 21<sup>st</sup> Century, with 19–23 models for each scenario. The resulting warming rate depended on the emissions scenario, and ranged from 0.16 K per decade for the scenario with the lowest emissions (B1), to 0.28 K per decade in the high emitting scenario (A2). In the intermediate emissions scenario (A1B) the warming rate was 0.23 K per decade.

For each scenario, the individual models produced different results. For the middle of the 21<sup>st</sup> Century, these inter-model differences were of similar magnitude as the differences between scenarios. The consensus between all simulations suggests a warming of 0–2 K during the first half of the 21<sup>st</sup> Century, with 1 K being the most likely temperature increase. For the latter part of the century the scenarios diverged. The CMIP-3 GCM results exhibited greater warming during winter than summer, with a difference of about half the annual warming (if annual warming was 2 K, then winter would warm by 1 K more than summer). Precipitation changes until the end of the 21<sup>st</sup> Century were found to range from 0.5–0.9% per decade. There is the possibility that precipitation might increase more during summer than winter, but individual model results varied substantially in this regard.

Several common threads stand out in regional climate change projections for Iceland. The rate of 21<sup>st</sup> Century warming in various GCMs on an annual basis varies from 0.2–0.3 K per decade, with more warming in winter than in summer. Precipitation is predicted to increase along with air temperature, with trends ranging between 0.5–1.8% per decade, but without consistent seasonal differences. Furthermore, the RCM results from the CE project showed enhanced warming in the interior and towards the northeast of Iceland. These model results, however, showed seasonal differences in warming rates that were inconsistent with other simulations.

To examine in more detail the various differences in regional climate predictions for Iceland in the 21<sup>st</sup> Century, specifically for future changes in surface air temperature (SAT) and total precipitation (TP), this study analyses several GCM simulations, together with those RCM runs, that were performed for the joint Climate and Energy Systems (CES) project of the Nordic countries (<http://en.vedur.is/ces>), which contributed data to Research Theme 3 (RT3), responsible for regional climate modelling research, of the Ensemble-based Predictions of Climate Changes and their Impacts (ENSEMBLES) project (van der Linden and Mitchell, 2009), funded by the European Commission under the 6<sup>th</sup> Framework Programme. Specific topics addressed in this study include spatial patterns of SAT and TP trends within the proximity of Iceland, such as land-sea differences and changes with terrain elevation, as well as seasonal differences. Additionally, the impact of driving GCMs on RCM runs will be investigated.

## 2 Data and Methodology

Data used in this study are monthly fields of surface (2m) air temperature (SAT) and total precipitation (TP), obtained from global as well as regional climate simulations.

The global data sets are 20<sup>th</sup> Century control runs, as well as 21<sup>st</sup> Century forecast runs, submitted by various institutions to the Intergovernmental Panel on Climate Change (IPCC) for their Forth

*Table 1. General circulation and regional climate models that were considered in this study.*

Model Version	Model Name, Institute
BCCR BCM 2.0	Bergen Climate Model, Bjerknes Centre for Climate Research, Bergen, Norway
CCCMA CGCM 3.1	Coupl. Glob. Clim. Mod., Canadian Centre for Climate Modelling and Analysis, Victoria
CSIRO MK 3.5	Glob. Clim. Mod., Commonwealth Scient. and Industrial Res. Organisation, Australia
MIROC 3.2 Medres	Model for Interdiscip. Res. on Clim., Division of Climate System Research, Tokyo, Japan
MIUB Echo G	Coupled Circulation Model, Meteorological Institute of the University of Bonn, Germany
MPI ECHAM5-r3	Global Climate Model, Max Planck Institute for Meteorology, Hamburg, Germany
MRI CGCM 2.3.2a	Coupled General Circulation Model, Meteorological Research Institute, Tsukuba, Japan
NCAR CCSM 3.0	Community Clim. Sys. Mod., National Center for Atmospheric Research, Boulder, USA
UKMO HadCM3	Hadley Centre Coupled Model, United Kingdom Meteorological Office, Exeter
UKMO HadGEM1	Hadley Centre Global Environ. Model, United Kingdom Meteorological Office, Exeter
SMHI-RCAO	Regional Atmos. Clim. Mod., Swedish Meteorol. and Hydrol. Institute, Norrköping
MetNo-HIRHAM	Regional Atmospheric Climate Model, Norwegian Meteorological Institute, Oslo
DMI-HIRHAM5	Regional Atmospheric Climate Model, Danish Meteorological Institute, Copenhagen

Assessment Report (IPCC, 2007). For the purpose of driving the 21<sup>st</sup> Century runs, the Special Report on Emissions Scenarios (SRES) originally prepared for the Third Assessment Report (IPCC, 2001), but also used in the Forth Assessment Report, defines a range of scenarios for future human activity and development. The A1B scenario used in this study assumes rapid world wide economic growth, a global population reaching 9 billion in 2050 and gradually declining afterwards, strong social interactions and converging prosperity worldwide, rapid development and spread of new technologies, and a balanced use of fossil and non-fossil energy sources.

The monthly fields from the various general circulation model (GCM) runs are interpolated onto a common  $2 \times 2$ -degree grid within the domain from  $10$ – $28^\circ$ W in longitude, and  $62$ – $68^\circ$ N in latitude, covering Iceland as the only land mass (see Fig. 1). To evaluate the accuracy of control runs, model results are compared with mean monthly fields on  $1 \times 1$ -degree grids obtained from the ERA-40 reanalysis project (Uppala et al., 2005). To that end, the 20<sup>th</sup> Century GCM runs are restricted to the 1958–98 control period, that is covered by all models, as well as the ERA-40 reanalyses.

To decrease the uncertainty of future climate scenarios for Iceland, the full set of 22 GCM runs was reduced to those ten models, that performed best for SAT during the 1958–98 control period, compared with the ERA-40 reanalyses. The performance of individual GCMs was measured by determining the root-mean-squared deviations from ERA-40 reanalyses of annual spatial mean values of SAT within the study domain. This selection procedure resulted in the ensemble of ten GCMs that are listed in Table 1. Given this reduced set of GCMs, the 21<sup>st</sup> Century IPCC forecast runs are restricted to the 2004–99 period, that is covered by all models.

In addition to the GCM runs, higher-resolution monthly fields of SAT and TP were obtained from those regional climate model (RCM) runs, that were recommended following the May 2009 CES staff meeting in Copenhagen (Kjellstöm, 2009). As indicated in Table 1, these are the MetNo-HIRHAM, downscaling the HadCM3; and the DMI-HIRHAM5 and SMHI-RCAO, downscaling ECHAM5-r3. For the latter, a special run over an extended Arctic domain was used (Koenigk

et al., 2011), rather than those that were provided to the ENSEMBLES project. Both driving GCMs are included in the reduced IPCC ensemble. Consistent with the GCM runs, also for the driving models of the RCM runs, the IPCC A1B emissions scenario was used. The monthly RCM fields are interpolated onto a common  $0.25 \times 0.25$ -degree grid within the same domain as the GCM fields.

Three 30-year climatological reference periods are used in this study: a 20<sup>th</sup> Century control period from 1961–90, as well as two future reference periods from 2021–50 and from 2070–99, respectively. Due to limited data availability, for the SMHI-RCAO run, the 20<sup>th</sup> Century control period is restricted to the 20-year period 1971–90, and the second 21<sup>st</sup> Century reference period is limited to the years of 2070–80. For the MetNo-HIRHAM runs, no data are available during the second 21<sup>st</sup> Century reference period.

### 3 Spatial Variability of Climate Trends

This section discusses the spatial patterns of long-term trends of surface air temperature and total precipitation, such as land-sea differences and changes with terrain elevation.

#### 3.1 Surface Air Temperature

Surface air temperature (SAT), as well as its changes over time, generally depend on surface type and terrain elevation. Specifically for the study domain, based on the climate simulations considered here, this is shown in Fig. 1. In the GCM ensemble mean field of SAT during the 1961–90 control period, the terrain of Iceland is recognised only by a weak wave pattern imposed on the larger-scale northwest to southeast gradient, resulting in about 2 K lower mean annual values over the land than over the surrounding ocean. By contrast, mean SAT fields in the RCM simulations show spatial patterns that are directly related to their respective model terrain (see Fig. 5 for the RCM orographies). As such, the spatial distribution of mean SAT is more realistic in the HIRHAM5 simulations than in the RCAO (see Fig. 2 for a comparison with the mean SAT field based on climate station data). However, all RCMs have mean annual SAT values that are consistent with long-term data records at the appropriate elevation of their model orography. As shown in Fig. 3 for the RCMs, the variability of SAT with ground elevation shows significant differences between the cold and warm season, with a marked change in the (pseudo-) vertical profile at around 300 mASL. Comparing summer and winter vertical profiles, the amplitude of the seasonal cycle in SAT increases from an average of 8 K near the coast to an average of 13 K between 300–600 m above mean sea level (mASL), and decreases gradually again at higher elevations. According to the Köppen classification scheme, this is indicative of the transition from a maritime to a continental subarctic climate at about an elevation of 300 mASL. The large increase in SAT from winter to summer at that level leads to decreasing lapse rates during the warm season at lower elevations, and increasing lapse rates above. The exact values are given in Table 2. Additionally, it can be seen from Fig. 3, that the spread of SAT values at each elevation, which is due to the northwest to southeast gradient over the surrounding ocean, decreases with height, especially in summer.

Table 2. Linear rates of decrease in SAT with terrain elevation (in Kelvin per kilometre) during the winter (DJF) and summer (JJA) months, over low ( $\leq 300$  mASL) and high ( $> 300$  mASL) terrain.

	Winter Low	Summer Low	Winter High	Summer High
SMHI-RCAO	12.1	1.7	5.2	5.3
MetNo-HIRHAM	23.0	-0.4	5.6	6.6
DMI-HIRHAM5	18.2	5.2	6.3	10.0

Correspondingly, as shown in Fig. 4, the largest seasonal cycle of SAT occurs in the low-lying interior of the island according to the RCM simulations. Additionally, despite the lower  $1 \times 1$ -degree resolution, a similar pattern is found in the reanalysis fields.

Referring again to Fig. 1, impacts of the terrain on linear trends of GCM ensemble mean SAT during the first half of the 21<sup>st</sup> Century are small. However, the RCMs predict an enhanced SAT increase during this period over the low-lying land area, compared with the surrounding ocean, especially the two HIRHAM runs. A more detailed analysis of linear 2004–50 SAT trends as a function of terrain elevation is given in Fig. 5. In the SMHI-RCAO and MetNo-HIRHAM runs, SAT trends increase with height up to about 600 m. Above that elevation and to the top of the terrain, trends remain constant in the SMHI-RCAO, but decrease slightly in the MetNo-HIRHAM. In the DMI-HIRHAM5, warming rates over the ocean and at low elevations are significantly higher, but decrease with height. However, these results are affected by what appears to be a spurious spatial SAT pattern east of Iceland (see Fig. 1). The DMI-HIRHAM5 results must therefore be interpreted with care in that regard, as will be discussed further below.

Comparing Figs. 1 and 6, these differences between the two HIRHAM runs, are largely due to different warming rates in their respective driving GCMs. However, even with the same driving GCM, the RCM responses may vary greatly.

The main difference between the HadCM3 and the ECHAM5 runs resides mostly in the location and timing of the largest SAT increase, rather than in the regional average of warming rate. Over the land and immediately to the north of Iceland, the HadCM3 is several degrees colder during the 1961–90 control period than the ECHAM5 (as well as the reduced IPCC ensemble mean). Subsequently, the largest SAT increase from the control period to the 2021–50 reference period, as well as the largest 2004–50 linear trends in the HadCM3 occur in that region. In contrast to that, in the ECHAM5, consistent with the reduced IPCC ensemble mean, the largest warming within the proximity of Iceland occurs along the southeast coast of Greenland in connection with sea ice reduction there. While these trends are physically motivated and consistent with past observed SAT trends based on the ERA-40 reanalyses (see Fig. 7), there is also a large SAT increase within a limited region to the northeast of Iceland, which is neither physically motivated nor consistent with past trends. Overall, however, SAT within the study domain, and its long-term changes there, are more realistically portrayed by the ECHAM5 than in the HadCM3, although not as well as by the reduced IPCC ensemble mean. Further differences between the HadCM3 and ECHAM5 exist in the timing of SAT increase, with the HadCM3 predicting larger warming during the second half of the 20th Century, relative to that during the first half of the 21<sup>st</sup> Century, than the ECHAM5.

These differences between the HadCM3 and the ECHAM5 simulations are also reflected in the corresponding RCM runs. Therefore, the MetNo-HIRHAM run, downscaling the HadCM3, is about 2–5 degrees colder over the northern part of Iceland during the control period than that of the DMI-HIRHAM5, downscaling the ECHAM5. For both RCMs, the largest warming in the driving GCM is outside the model domain. However, in the case of the DMI-HIRHAM5, the large warming in the ECHAM5 to the northeast of Iceland is amplified by the RCM. Consequently, the overall warming rates over the ocean and at low elevations, especially in the northeast of Iceland, are significantly larger in the DMI-HIRHAM5 than in any of the other RCMs, including the SMHI-RCAO, which is forced by the same GCM. This implies that the dependence of warming rate on terrain elevation, as depicted by the DMI-HIRHAM5, must be considered with care.

Similarly, differences in the timing of SAT increase between the RCM simulations are carried over from their driving GCMs, with the MetNo-HIRHAM experiencing larger warming during the second half of the 20th Century, relative to that during the first half of the 21<sup>st</sup> Century, than the DMI-HIRHAM5.

As shown in Fig. 8, the degree to which GCM trends are reproduced depends on the RCM. As noted above, the strong amplification by the DMI-HIRHAM5 of the spurious warming to the east of Iceland in the ECHAM5 is absent in the SMHI-RCAO. Similarly, in the MetNo-HIRHAM the suspicious enhancement of warming in the HadCM3 to the north of Iceland is reduced.

### 3.2 Total Precipitation

As with surface air temperature (SAT), total precipitation (TP) depends on surface type and terrain elevation (see Fig. 9). Similarly to SAT, the terrain of Iceland only induces a weak wave pattern in the larger-scale northeast to southwest gradient in the GCM ensemble mean field of TP during the 1961–90 control period, resulting in about 0.5 mm day<sup>-1</sup> lower mean annual values over the land than over the surrounding ocean. By contrast, mean TP fields in the RCM simulations show spatial patterns that are directly related to their respective model terrain (see again Fig. 5 for the RCM orographies). As such, the spatial distribution of mean TP is more realistic in the HIRHAM simulations than in the RCAO (see again Fig. 2 for a comparison with the mean TP field based on climate station data). Of the two HIRHAM runs, the one conducted by MetNo based on the HadCM3 is significantly closer to the observed TP field during the control period. As shown in Fig. 10, in the DMI-HIRHAM5, in contrast with the reanalyses and the other RCMs, the Icelandic Low is to the southeast of Iceland and more intense. The prevailing surface winds, therefore, have a northeasterly direction across the study domain, compared with easterly or southeasterly directions as found in the reanalyses and the other RCMs. These special wind conditions result in enhanced precipitation over the eastern part of Iceland, compared with observations and the MetNo-HIRHAM run.

Contrary to SAT, in the RCMs, the rate of change of TP with ground elevation does not show consistent differences between the cold and warm season, with a larger variability at each elevation, to the extent that the calculation of meaningful (pseudo-) vertical profiles is not possible (see again Fig. 3).

Referring again to Fig. 9, impacts of the terrain on linear trends of GCM ensemble mean TP

during the first half of the 21<sup>st</sup> Century are small. Moreover, in contrast to SAT, also the RCMs, with the exception of the DMI-HIRHAM5, do not predict significantly different TP trends during this period over the low-lying land area, compared with the surrounding ocean. In the case of the DMI-HIRHAM5, there is a dipole pattern across Iceland, with increasing TP in the northeast, and decreasing TP in the southwest.

A more detailed analysis of linear 2004–50 TP trends as a function of terrain elevation is given in Fig. 11. In the SMHI-RCAO, contrary to the HIRHAM5 runs, TP trends decrease with height. In the MetNo-HIRHAM, TP is predicted to decrease below 1 km elevation, with an increase above that level. In the DMI-HIRHAM5, TP trends over the land are positive above an elevation of 400 m. Thus it appears that no definite conclusions can be drawn regarding the variation of precipitation trends with elevation based on these simulations.

Comparing Figs. 9 and 12, these differences between the two HIRHAM5 runs, are largely due to different TP trends in their respective driving GCMs. In connection with the large warming that is predicted by the ECHAM5 within a limited region to the east of Iceland, there is also a large increase in TP in the same area over the first half of the 21<sup>st</sup> Century. This is inconsistent with past TP trends derived from the ERA-40 reanalyses, despite the fact that the mean TP field during the 1961–90 control period in the ECHAM5 was very close to the mean reanalysis field, and closer than in the HadCM3 (see again Fig. 7). However, just as with the large SAT increase, the large TP trends at the eastern edge of the study domain are neither physically motivated nor consistent with past trends, and are therefore most likely a model artefact. As with SAT, this artificially large increase in TP is reproduced by the DMI-HIRHAM5. However, the HadCM3, and in fact the reduced IPCC ensemble mean, are likely to have shortcomings as well, with regard to the spatial distribution of TP trends within the study domain. This is suggested by the inconsistency between predicted TP trends during the first half of the 21<sup>st</sup> Century, and those found in the ERA-40 reanalyses, leading up to the beginning of the 21<sup>st</sup> Century. In fact, the reduced IPCC ensemble mean suggests a shift in the region of the largest increase in TP from south of Iceland, as demonstrated by the reanalyses for the second half of the 20th Century, to the north for the following 50 years. Both the GCM as well as RCM predictions of the spatial pattern of TP change within the study domain are therefore highly uncertain, and likely to reflect mostly natural variability of precipitation in the area.

As shown in Fig. 13, similarly to the spatial distribution of SAT trends, the SMHI-RCAO and the MetNo-HIRHAM have a tendency to reduce the magnitude of extrema in the respective GCM fields of TP, whereas the spatial patterns in the ECHAM5 are further enhanced by the DMI-HIRHAM5.

## **4 Long-Term Trends of Annual Mean Values**

In this section, the variability and long-term trends of annual and regional mean values of surface air temperature and total precipitation are analysed.

For the GCM runs, a distinction is made between ocean and land areas, based on whether a grid



Table 3. Number of grid points of interpolated fields within the study domain for the different models in different zones.

	Ocean	Land	Low Terrain	High Terrain	Entire Domain
IPCC GCMs	32	8	–	–	40
SMHI-RCAO	1461	364	102	262	1825
MetNo-HIRHAM	1465	314	78	236	1779
DMI-HIRHAM5	1487	301	78	223	1788

point is outside or within the actual boundaries of Iceland. For the RCM runs, the land area is additionally divided into low terrain up to 300 metres above mean sea level (mASL), and high terrain above 300 mASL. To determine the elevation at each grid point, the respective model orography (rather than real terrain elevation) was used. The numbers of grid points in each zone are given in Table 3.

#### 4.1 Surface Air Temperature

A graphic representation of the evolution of annual mean values of surface air temperature (SAT) over the entire land area of Iceland is given in Fig. 14. Due to the elevated terrain, mean SAT in the RCM runs is lower than in most of the GCM runs within in the reduced IPCC ensemble considered here. However, the RCM mean values are similar to each other at the beginning of the 21<sup>st</sup> Century, and converge further as time progresses. During the control period, the ensemble mean, as well as the SMHI-RCAO and the DMI-HIRHAM5 are close to the ERA-40 reanalyses, with only the MetNo-HIRHAM, reproducing the cold bias of the HadCM3, being significantly colder.

As shown in Fig. 15, taking into account all RCM simulations included in the RT2B transient experiments of the ENSEMBLES project (see <http://ensemblesrt3.dmi.dk>), results in somewhat larger SAT trends from about 1970 onwards, due to the low ensemble mean SAT values during the 1961–90 control period.

The exact values of linear SAT trends, determined by least-squares regression, are given in Table 4. Based on a standard t-test, all these trends are significantly different from zero on the 99.9% confidence level. As seen before, based on the reduced IPCC ensemble mean, differences in linear SAT trends over the ocean and the land are small, being 0.30 and 0.31 K per decade, respectively, for the 2004–50 period. In the RCMs, land-sea differences are larger, with an average SAT trend for the 2004–50 period of 0.27 K per decade over the ocean, and 0.31 K per decade over the land. Although, on average, SAT trends over the ocean are somewhat smaller in the RCMs than in the GCMs, the ensemble mean warming rates in the RCMs and GCMs over the land are identical. As discussed previously, the DMI-HIRHAM5 results are suspect with regard to spatial variability of SAT trends. However, from the other two RCM simulations, relative enhancement of warming between the surrounding sea area and the Icelandic highlands can be determined. It is found that, according to the SMHI-RCAO, this enhancement is 24%, and 46% for the MetNo-HIRHAM. A conservative enhancement of the reduced IPCC ensemble mean warming rate would therefore result in 0.37 K per decade for the Icelandic elevated terrain.

Table 4. Linear trends of surface air temperature in Kelvin per decade between specific years in different zones (ocean / land / low terrain / high terrain).

	2004–50	2004–80	2004–99
IPCC GCM Mean	0.30 / 0.31 / - / -	0.28 / 0.29 / - / -	0.23 / 0.24 / - / -
SMHI-RCAO	0.17 / 0.19 / 0.18 / 0.21	0.17 / 0.21 / 0.20 / 0.24	–
MetNo-HIRHAM	0.24 / 0.32 / 0.29 / 0.35	–	–
DMI-HIRHAM5	0.40 / 0.43 / 0.44 / 0.43	0.31 / 0.36 / 0.37 / 0.35	0.29 / 0.34 / 0.35 / 0.33

Table 5. Average linear trends of surface air temperature in Kelvin per decade with randomised beginning and end years in different zones (ocean / land / low terrain / high terrain). Actual beginning and end years vary between  $\pm 5$  years relative to those given.

	2009–45	2009–75	2009–94
IPCC GCM Mean	0.28 / 0.31 / - / -	0.28 / 0.30 / - / -	0.25 / 0.27 / - / -
SMHI-RCAO	0.13 / 0.18 / 0.17 / 0.19	0.18 / 0.24 / 0.22 / 0.25	–
MetNo-HIRHAM	0.24 / 0.32 / 0.30 / 0.33	–	–
DMI-HIRHAM5	0.49 / 0.55 / 0.58 / 0.55	0.35 / 0.40 / 0.43 / 0.40	0.32 / 0.38 / 0.40 / 0.37

To eliminate biases in SAT trends, that might be the result of the specific beginning and end dates used in these regression analyses, linear SAT trend values were also calculated for 1000 time-series with randomised beginning and end years within a 10-year range centred around the fixed beginning and end years. This analysis was repeated 10 times, and the mean values of each set of randomised trends, as well as their standard deviations, are given in Tables 5 and 6, respectively, up to that precision at which all of the 10 realisations result in the same mean value. With the exception of the DMI-HIRHAM5, differences between linear trends with either specific or randomised beginning and end years are small. However, in the DMI-HIRHAM5, the specific years chosen, especially for the 2004–50 period, result in linear SAT trends, which are significantly lower compared with similar beginning and end years. Consequently, for the 2004–50 period, the average RCM warming rates of 0.29 K per decade over the ocean, and 0.35 K per decade over the land are somewhat larger than for the reduced IPCC ensemble mean.

Additionally, the tabulated values of SAT differences between the 1961–90 control period and either the 2021–50 or the 2070–99 reference period are given in Table 7. The relatively small changes in mean SAT values from the control to the first reference period, compared with the linear trends over the 2004–50 period, in the SMHI-RCAO and to some extent also in the DMI-HIRHAM5, are due to the comparatively high annual mean values during the control period (see again Fig. 14).

Table 6. Standard deviations of randomised linear trends of surface air temperature in Kelvin per decade  $\times 10^{-2}$  in different zones (ocean / land / low terrain / high terrain).

	2009–45	2009–75	2009–94
IPCC GCM Mean	2.8 / 2.7 / - / -	0.5 / 0.5 / - / -	1.2 / 1.2 / - / -
SMHI-RCAO	3.5 / 3.6 / 3.5 / 3.7	1.1 / 1.3 / 1.3 / 1.3	–
MetNo-HIRHAM	1.8 / 4.7 / 3.3 / 5.2	–	–
DMI-HIRHAM5	8.2 / 10.4 / 10.7 / 10.2	1.9 / 2.3 / 2.4 / 2.2	1.1 / 1.4 / 1.4 / 1.4

Table 7. Changes in surface air temperature from the 1961–90 control period to the 2021–50 reference period ( $\Delta T_1$ ) or the 2070–99 reference period ( $\Delta T_2$ ) in different zones (ocean / land / low terrain / high terrain).

	$\Delta T_1$	$\Delta T_2$
IPCC GCM Mean	1.3 / 1.3 / - / -	2.4 / 2.6 / - / -
SMHI-RCAO	0 / 0.3 / 0.2 / 0.4	0.6 / 1.2 / 1.0 / 1.3
MetNo-HIRHAM	1.8 / 2.1 / 2.0 / 2.1	–
DMI-HIRHAM5	1.0 / 1.0 / 1.0 / 1.0	2.2 / 2.6 / 2.6 / 2.6

## 4.2 Total Precipitation

Referring again to Fig. 14, the annual mean values of total precipitation (TP) over the entire land area of Iceland in the ERA-40 reanalyses, as well as the RCM runs, fluctuate strongly from one year to the next. In fact, based on a standard t-test, linear TP trends in reanalyses and RCM runs, determined by least-squares regression, are significantly different from zero only well below the 90% confidence level. The resulting linear trends are therefore omitted from this analysis. However, the long-term TP trends for the reduced IPCC ensemble mean are significant on the 99.9% level, and are given in Table 8, both for specific as well as randomised beginning and end dates, as described in the previous section. Also given in parentheses are the shorter-term TP trends, which are significant on the 95% confidence level. Over the longer periods, linear TP trends over the ocean are robust with respect to changing beginning and end years. Over the land, there is a 10% difference between trends with either specific or randomised beginning and end years.

Additionally, the tabulated values of TP differences between the 1961–90 control period and either the 2021–50 or the 2070–99 reference period are given in Table 9.

Finally, the ratios of linear trends of TP over SAT for statistically significant TP trends between specific beginning and end dates are given in Table 10. Differences between trend ratios with specific or randomised beginning and end years over the longer periods are small. As the length of the time period increases, the increase in TP per degree warming over the land relative to the ocean gets larger. Therefore, towards the end of the 21<sup>st</sup> Century over the land, there is a proportionally larger increase in TP compared with SAT than during the first half of the Century.

Table 8. Linear trends of total precipitation in percent of the 1961–90 average per decade between specific years in different zones (ocean / land) based on the IPCC GCM mean.

	2004–50	2004–80	2004–99
Specific Years	(0.8) / (0.8)	0.8 / 1.0	0.7 / 1.0
Randomised Years	(1.0) / (1.0)	0.8 / 1.1	0.7 / 1.1
Standard Deviation	0.30 / 0.32	0.08 / 0.11	0.06 / 0.06

Table 9. Changes in total precipitation from the 1961–90 control period to the 2021–50 reference period ( $\Delta P_1$ ) or the 2070–99 reference period ( $\Delta P_2$ ) in different zones (ocean / land / low terrain / high terrain), in units of percent of the 1961–90 average.

	$\Delta P_1$	$\Delta P_2$
IPCC GCM Mean	4.4 / 3.9 / - / -	8.1 / 10.0 / - / -
SMHI-RCAO	0.2 / 1.1 / 2.8 / 0.4	5.2 / 5.8 / 9.8 / 4.3
MetNo-HIRHAM	4.3 / 4.3 / 4.3 / 4.3	–
DMI-HIRHAM5	2.4 / 2.8 / 2.4 / 3.0	1.9 / 7.6 / 6.2 / 8.1

Table 10. Ratios of linear trends of total precipitation over surface air temperature in percent of the 1961–90 average per Kelvin of surface air warming between specific years in different zones (ocean / land) based on the IPCC GCM mean.

	2004–50	2004–80	2004–99
Specific Years	2.7 / 2.6	2.9 / 3.4	3.0 / 4.2
Randomised Years	3.6 / 3.2	2.9 / 3.7	2.8 / 4.1

## 5 Seasonal Differences in Climate Trends

The seasonal cycle for Iceland of surface air temperature (SAT) and total precipitation (TP) based on monthly mean values over the land area is graphically represented in Fig. 16. Although the absolute values differ somewhat between the reduced IPCC ensemble mean and the three RCM runs, the timing of the maximum and minimum values is similar. Maximum SAT values occur in July or August, with minimum values in January or February. Maximum TP values occur in October or November, while minimum values are found in May or June.

However, as shown in Fig. 17, there are no consistent seasonal differences between the GCM ensemble mean and the individual RCM runs in changes of mean monthly SAT and TP values from the 1961–90 control period to either the 2021–50 or the 2070–99 reference period. However, for SAT, the consensus is such that greater warming is predicted for the cold than for the warm season, whereby the difference between the largest warming in February and the smallest warming in June doubles from 0.8 K between the control and the first reference period, to 1.6 K between the control and the second reference period. Based on the differences between the control and

the second reference period, the SMHI-RCAO also shows increased warming from November through January, while the DMI-HIRHAM5 over that same period predicts a somewhat enhanced SAT increase in January, compared with the rest of the year. Over shorter periods and for TP, there is no well defined seasonal cycle in mean monthly changes.

To test the representativeness of the three main RCMs that were chosen for this study, a similar analysis was performed including all RCMs that contributed continuous monthly data over the 1951–2100 period to the RT2B transient experiments of the ENSEMBLES project, both with 25 and 50 km resolution (see <http://ensemblesrt3.dmi.dk>). All of these RCM runs were forced by GCM simulations based on the IPCC A1B emissions scenario.

The results, separated by driving GCM, are shown in Fig. 18. Most RCMs predict less warming over Iceland in the summer months from June to August than during the rest of the year. However, as with the spatial distribution of SAT trends, the driving GCMs also have a dominant impact on the seasonal cycle of warming rate. Therefore, the time of year with the largest warming depends on the underlying GCM simulations. Those RCMs that are downscaling HadCM3, predict the largest SAT increase to occur between January and March, whereas most RCMs that are downscaling ECHAM5, predict the greatest warming to occur in November, with a secondary maximum in February or March.

## 6 Conclusions

It was demonstrated by comparison between GCM fields on a  $2 \times 2$ -degree grid, ERA-40 reanalyses on a  $1 \times 1$ -degree grid, RCM simulations on a  $0.25 \times 0.25$ -degree grid, and high-density observations, that a spatial resolution better than  $1^\circ$  in longitude and latitude is essential for an accurate representation of surface air temperature (SAT) and total precipitation (TP) over the complex terrain of Iceland. A comparison between the SMHI-RCAO and the two versions of HIRHAM shows that a higher resolution is only useful for a more accurate simulation of surface variables, if the terrain on the resolved scale is realistically represented. Furthermore, a comparison between the MetNo-HIRHAM and the DMI-HIRHAM5 shows that, even with appropriate terrain, for a realistic spatial distribution of TP also the large-scale wind conditions need to be accurately represented.

In addition to the general problems associated with climate predictions on any spatial scale, regional climate predictions for Iceland are further complicated by its location between the large ice sheet of Greenland to the northwest and the warm surface waters of the North Atlantic Current to the southeast. Within that region, the possibility of land and sea ice melting, together with potential changes in the ocean circulation, lead to strong responses in most of the GCMs with regard to SAT and TP over the course of the 21<sup>st</sup> Century. However, comparing different GCM simulations, there are large uncertainties in the magnitude and the timing of these events.

As shown here, both for the spatial distribution and the seasonal cycle of SAT and TP trends, RCM simulations are strongly influenced by their driving GCMs. Even if during the control period the RCM field is significantly improved compared with the large-scale GCM field, and in fact highly accurate compared with observations, during the subsequent forecast runs, the RCMs strongly

depend on their driving GCMs, such that changes over time are dominated by the larger-scale climate trends in the GCM. At low elevations and over the ocean, RCMs therefore provide little independent information beyond the GCM results. Moreover, they carry over the largest errors from the global simulations.

These results show the limitations of pure dynamical downscaling. At least over the first half of 21<sup>st</sup> Century, the reliability of RCM results may be increased if constraints from the past climatology are taken into account. In this way, the impact of climate trends in GCMs, that are inconsistent with recent past trends, might be minimised. Examples of these are the large warming and increase in precipitation in the ECHAM5 in a region northeast of Iceland, or the reversal of the north-south gradient across the island in TP trends in the majority of GCMs considered here.

However, assuming that the IPCC A1B emissions scenario used in this study is realistic, there are already several predictions that can be made with a high degree of certainty, based on the future climate scenarios available at the moment. For example, it is clear from both the GCM and RCM ensemble means, that SAT is likely to increase at a rate close to 0.3 K per decade until 2050, both over the land and nearby surrounding ocean, with superimposed decadal variations determined by natural climate variability. More precisely, it seems likely that the warming rate over land will be in the approximate range of 0.2–0.4 K per decade, with a somewhat smaller trend of 0.15–0.30 K per decade over the ocean. If, as assumed in the A1B scenario, global population and CO<sub>2</sub> emissions decrease after 2050, the reduced IPCC ensemble used in this study predicts that SAT will increase at a reduced rate of about 0.2 K per decade in the second half of the 21<sup>st</sup> Century. With TP, inter-annual fluctuations and inter-model differences are significantly larger than for SAT. However, based on the reduced IPCC ensemble, it is likely that TP will increase at a rate of about 1% of the 1961–90 average per decade throughout the 21<sup>st</sup> Century, with somewhat lower trends over the ocean than over the land area.

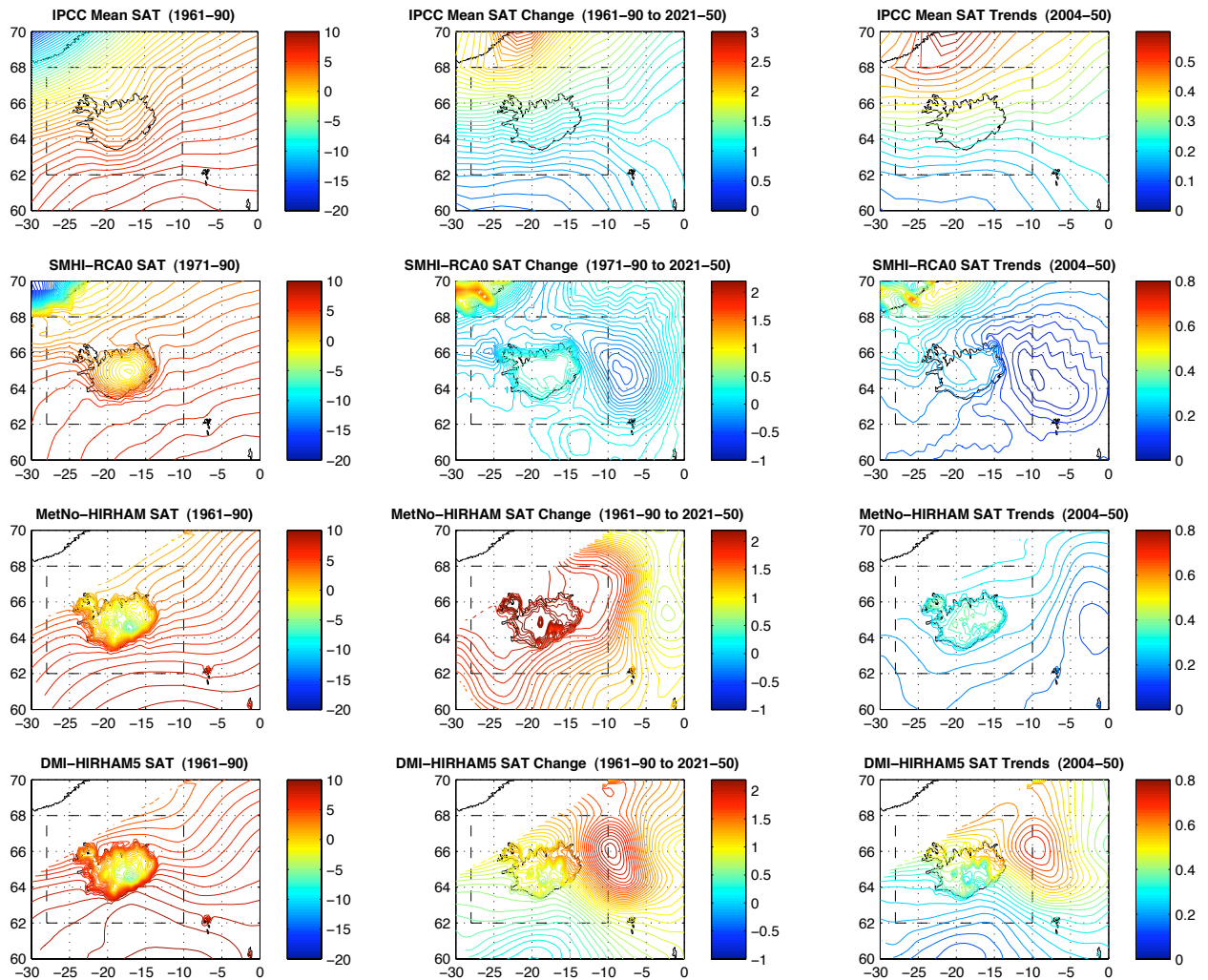


Figure 1. Mean annual surface air temperature (SAT) in degrees centigrade during the 1961–90 control period (left column), differences in degrees between the control period and the 2021–50 reference period (centre column), and linear trends in degrees per decade within the 2004–50 period (right column), for the IPCC GCM ensemble mean (top row), the SMHI-RCA0 (second row from top), the MetNo-HIRHAM (second row from bottom), and the DMI-HIRHAM5 (bottom row). The dashed lines indicate the study domain.

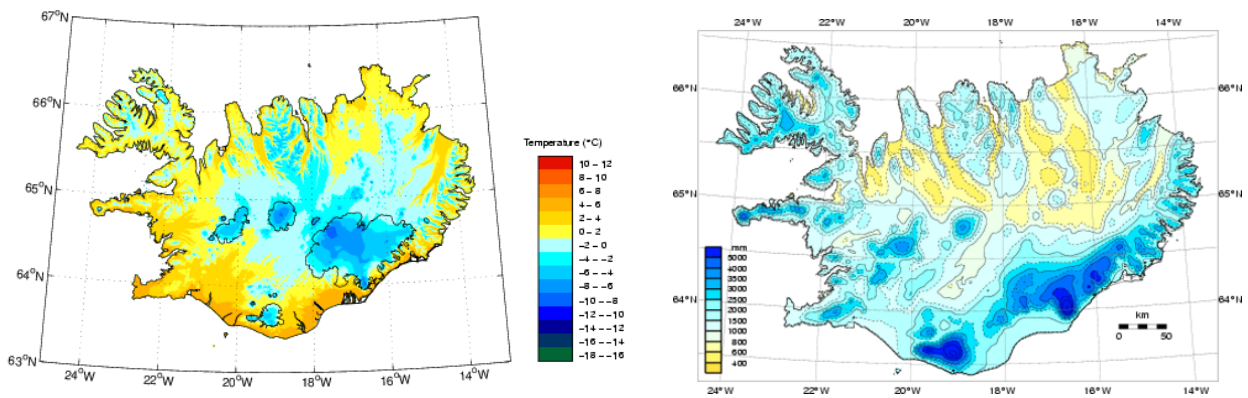


Figure 2. Mean annual surface air temperature (left panel) and total precipitation (right panel) during the 1961–90 control period. Maps were retrieved on 20 April 2010 from the Icelandic Meteorological Office; available online at: <http://andvari.vedur.is/vedurfar/vedurfarsmyndir/EV.DTO/ann.html>, originally published by Björnsson et al. (2007); and [http://www.vedur.is/vedur/vedurfar/kort/medalurkoma\\_arsins](http://www.vedur.is/vedur/vedurfar/kort/medalurkoma_arsins), originally published by Crochet et al. (2007).



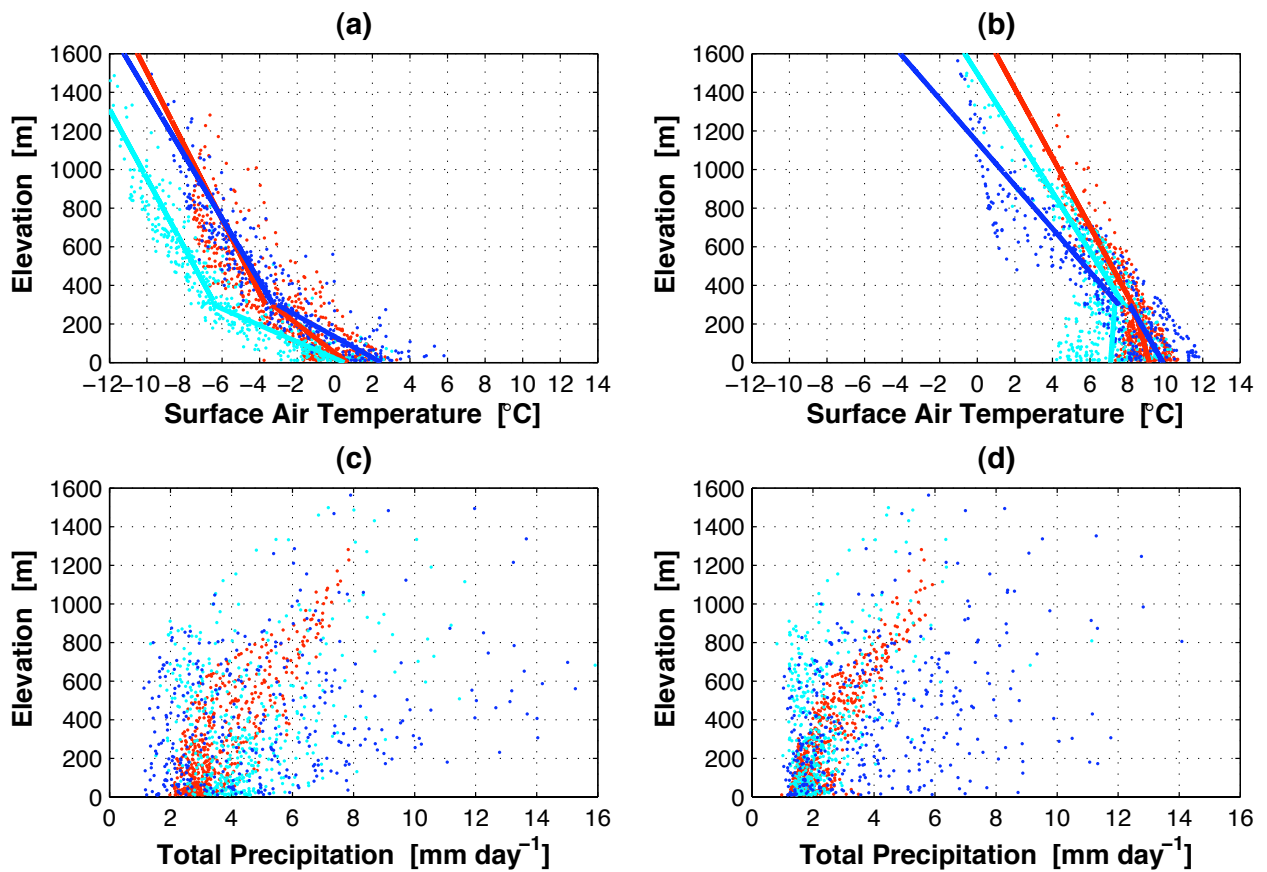


Figure 3. Dependence on terrain elevation of surface air temperature ((a) and (b)) and total precipitation ((c) and (d)) in the RCMs (SMHI-RCAO, red; MetNo-HIRHAM, cyan; DMI-HIRHAM5, blue) during the 1961–90 control period in winter (DJF; (a) and (c)) and summer (JJA; (b) and (d)).

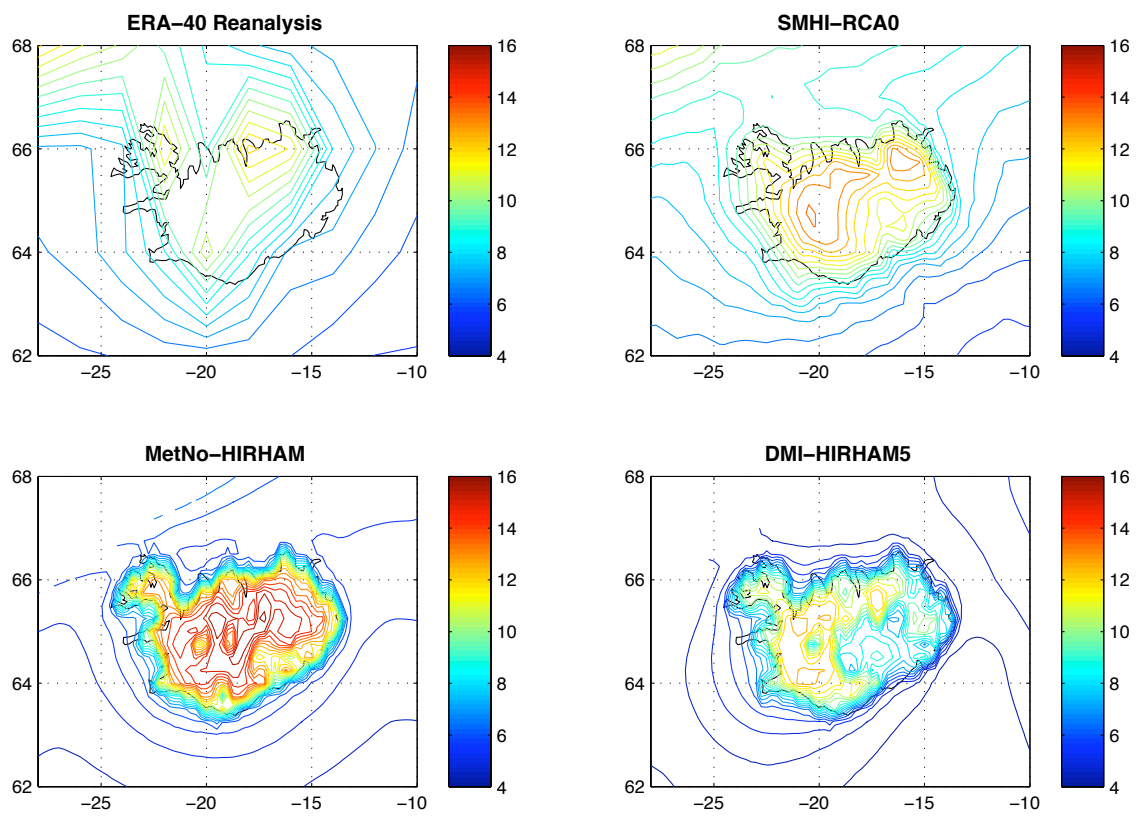


Figure 4. Differences between summer (JJA) and winter (DJF) mean seasonal surface air temperature in degrees centigrade during the 1961-90 control period, for the reanalyses and the RCMs.

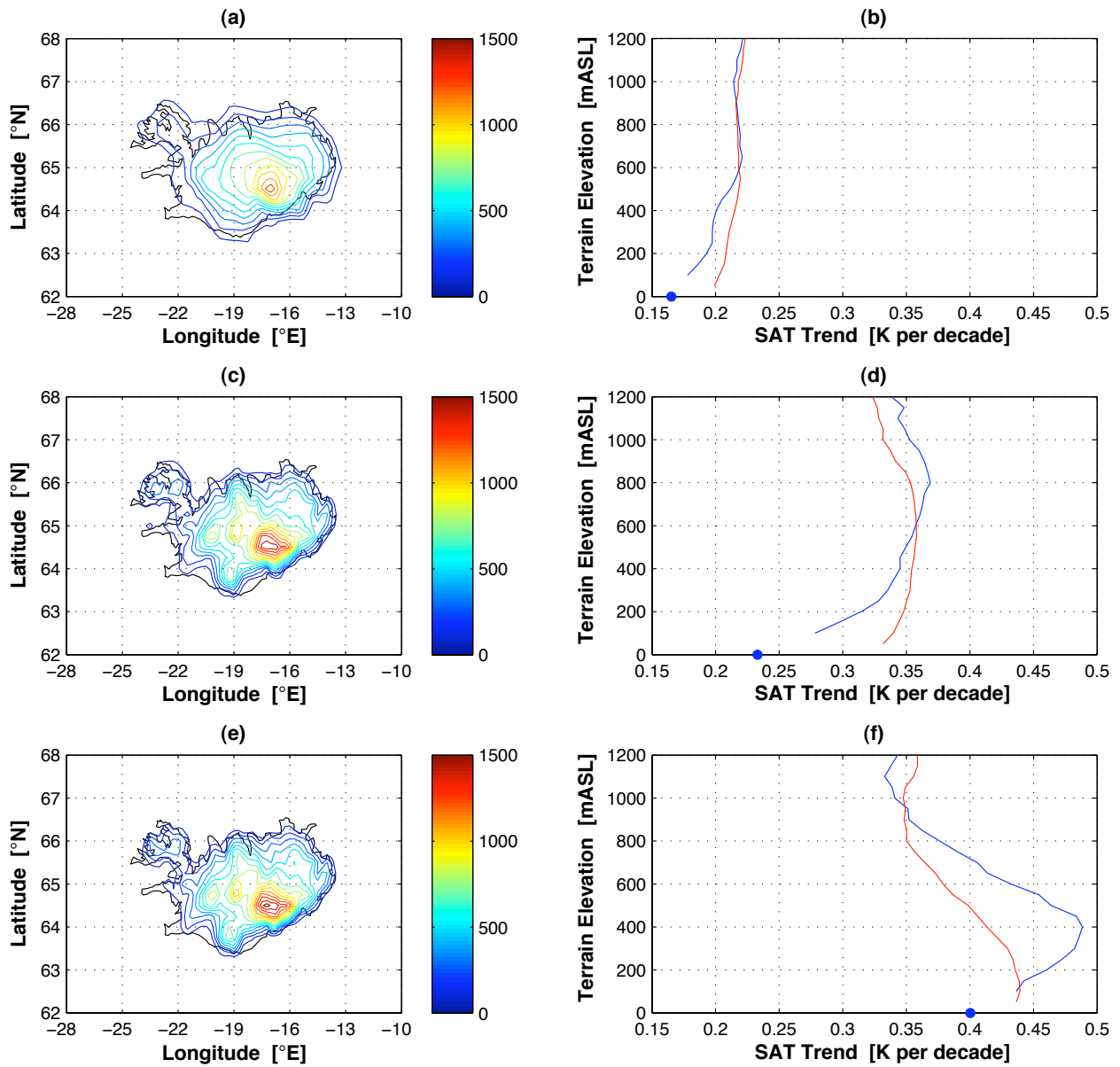


Figure 5. Dependence on terrain elevation of linear trends of surface air temperature within the 2004–50 period in (b) the SMHI-RCAO, (d) the MetNo-HIRHAM, and (f) the DMI-HIRHAM5, together with the corresponding model orographies in (a), (c), and (e), respectively. The blue dots indicate mean values over the ocean within the domains shown on the left. The blue lines indicate mean values at the given elevation, whereas the red lines indicate mean values at or above the given elevation.

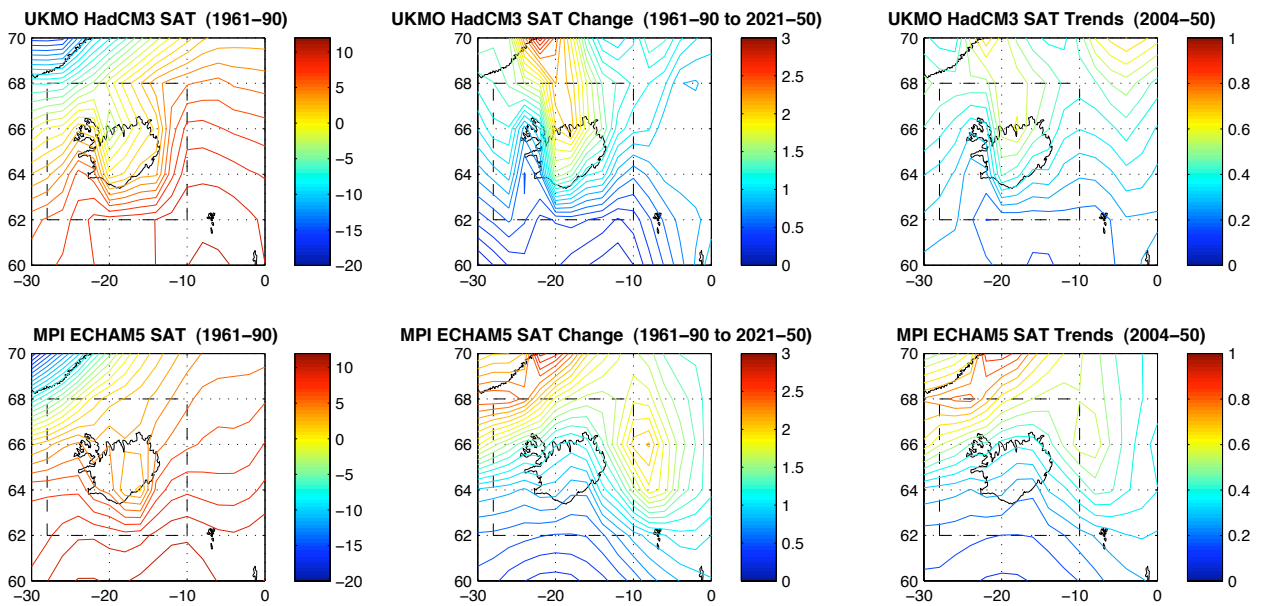


Figure 6. Mean annual surface air temperature (SAT) in degrees centigrade during the 1961–90 control period (left column), differences in degrees between the control period and the 2021–50 reference period (centre column), and linear trends in degrees per decade within the 2004–50 period (right column), for the UKMO HadCM3 (top row), and the MPI ECHAM5-r3 (bottom row). The dashed lines indicate the study domain.

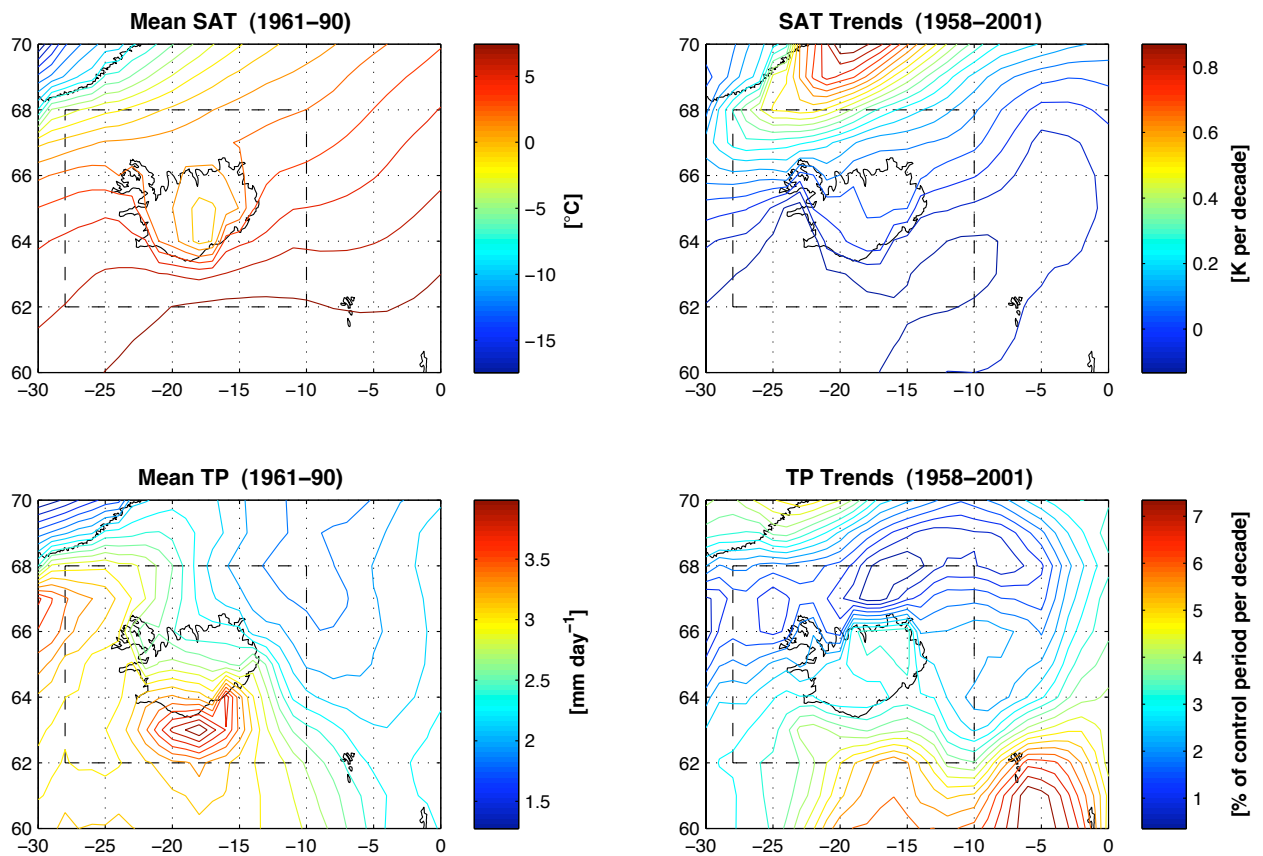


Figure 7. Mean annual surface air temperature (SAT) and total precipitation (TP) during the 1961–90 control period, and linear trends within the 1958–2001 period, for the ERA-40 reanalyses. The dashed lines indicate the study domain.

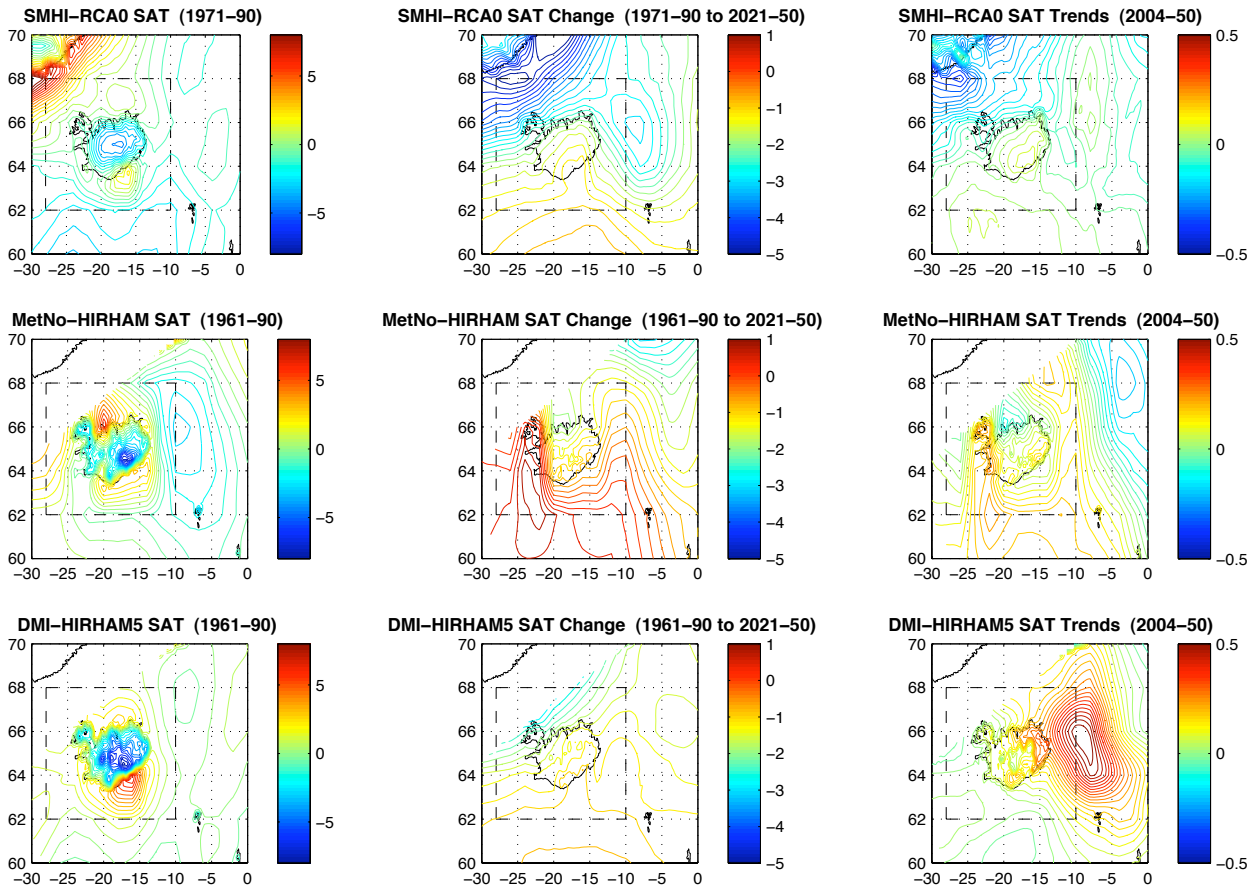


Figure 8. Differences between the RCM and underlying GCM simulations of mean annual surface air temperature (SAT): mean fields in degrees centigrade during the 1961–90 control period (left column), differences in degrees between the control period and the 2021–50 reference period (centre column), and linear trends in degrees per decade within the 2004–50 period (right column), for the SMHI-RCA0 (top row), the MetNo-HIRHAM (middle row), and the DMI-HIRHAM5 (bottom row). The dashed lines indicate the study domain.

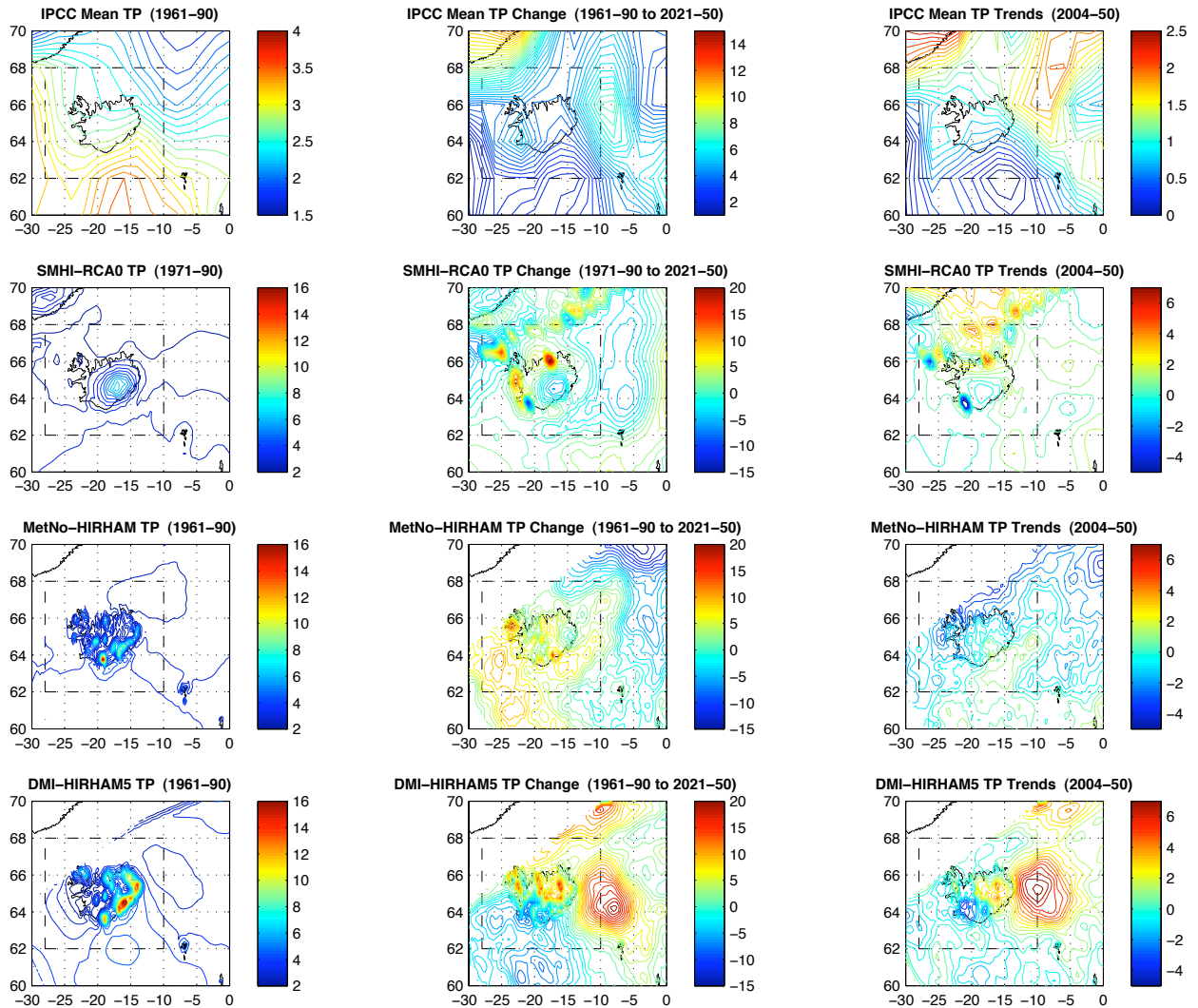


Figure 9. Mean annual total precipitation (TP) in millimetres per day during the 1961–90 control period (left column), differences in percent of the control period between the control period and the 2021–50 reference period (centre column), and linear trends in percent of the control period per decade within the 2004–50 period (right column), for the IPCC GCM ensemble mean (top row), the SMHI-RCA0 (second row from top), the MetNo-HIRHAM (second row from bottom), and the DMI-HIRHAM5 (bottom row). The dashed lines indicate the study domain.



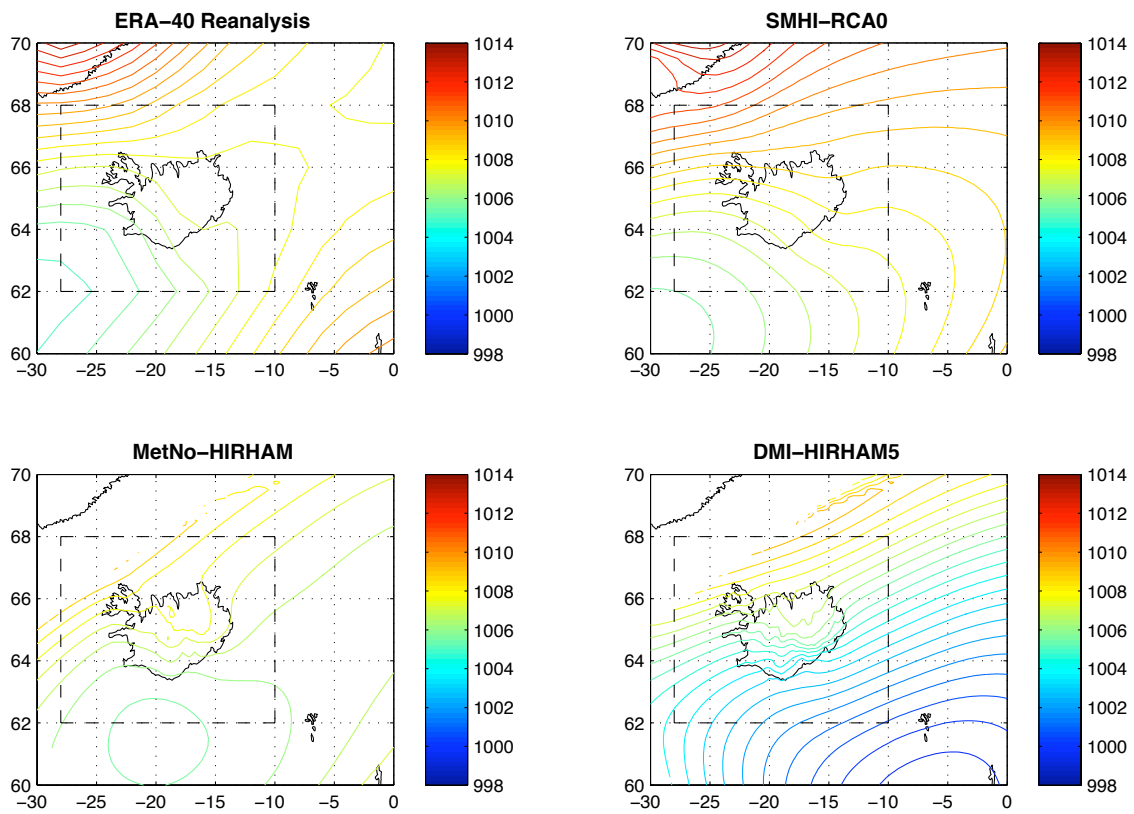


Figure 10. Mean annual air pressure at mean sea level in hectopascals during the 1961–90 control period, for the reanalyses and the RCMs. The dashed lines indicate the study domain.



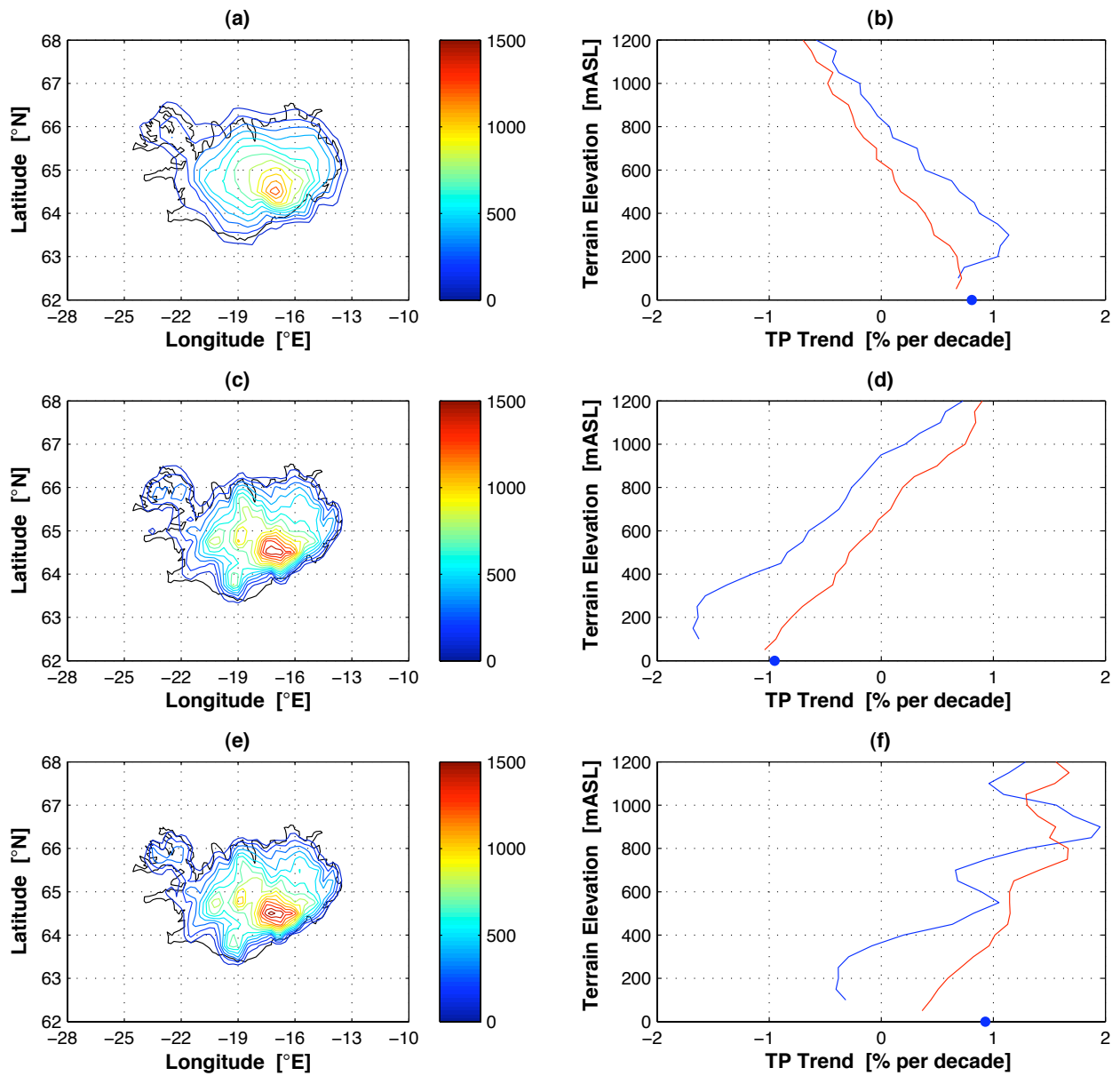


Figure 11. Dependence on terrain elevation of linear trends of total precipitation within the 2004–50 period in (b) the SMHI-RCAO, (d) the MetNo-HIRHAM, and (f) the DMI-HIRHAM5, together with the corresponding model orographies in (a), (c), and (e), respectively. The blue dots indicate mean values over the ocean within the domains shown on the left. The blue lines indicate mean values at the given elevation, whereas the red lines indicate mean values at or above the given elevation. As discussed in Section 4, the DMI-HIRHAM5 results must be seen as suspect in that regard.

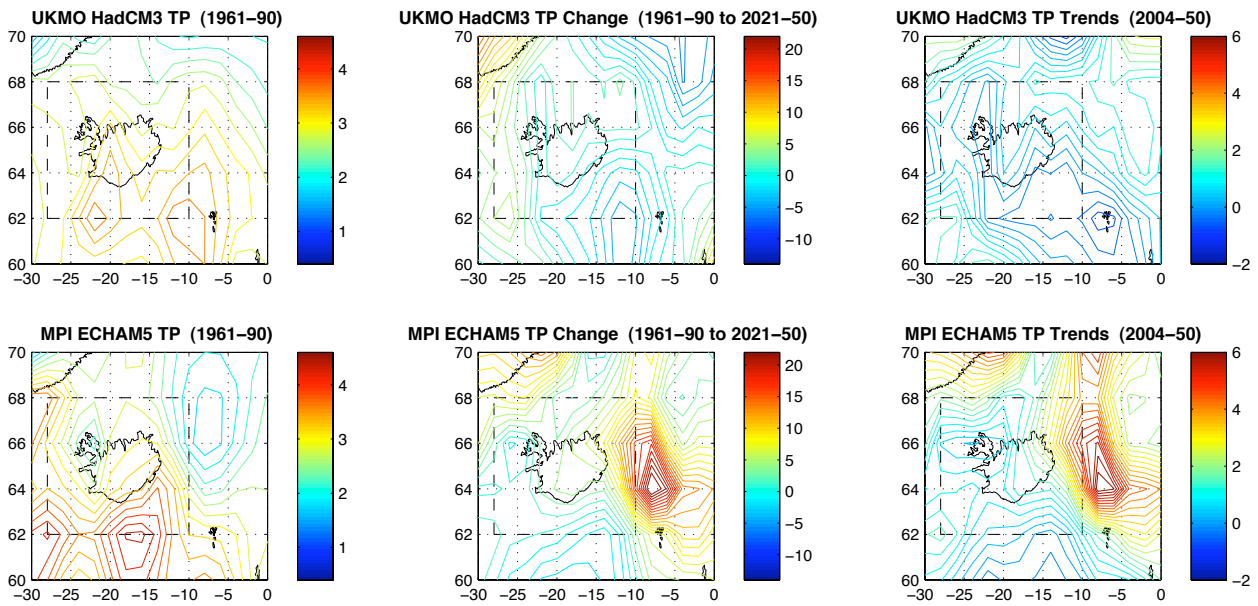


Figure 12. Mean annual total precipitation (TP) in millimetres per day during the 1961–90 control period (left column), differences in percent of the control period between the control period and the 2021–50 reference period (centre column), and linear trends in percent of the control period per decade within the 2004–50 period (right column), for the the UKMO HadCM3 (top row), and the MPI ECHAM5-r3 (bottom row). The dashed lines indicate the study domain.

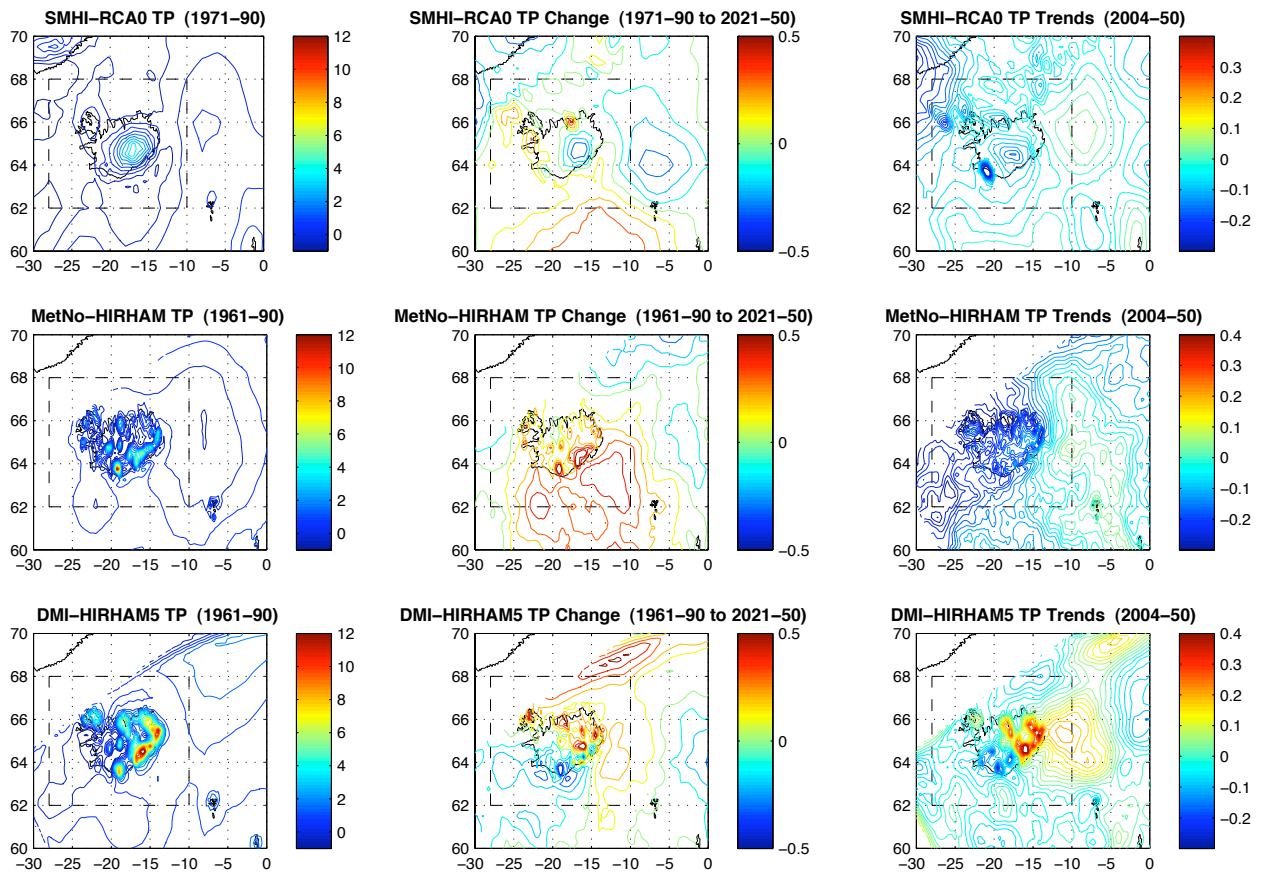


Figure 13. Differences between the RCM and underlying GCM simulations of mean annual total precipitation (TP): mean fields in millimetres per day during the 1961–90 control period (left column), differences in millimetres per day between the control period and the 2021–50 reference period (centre column), and linear trends in millimetres per day per decade within the 2004–50 period (right column), for the SMHI-RCA0 (top row), the MetNo-HIRHAM (middle row), and the DMI-HIRHAM5 (bottom row). The dashed lines indicate the study domain.

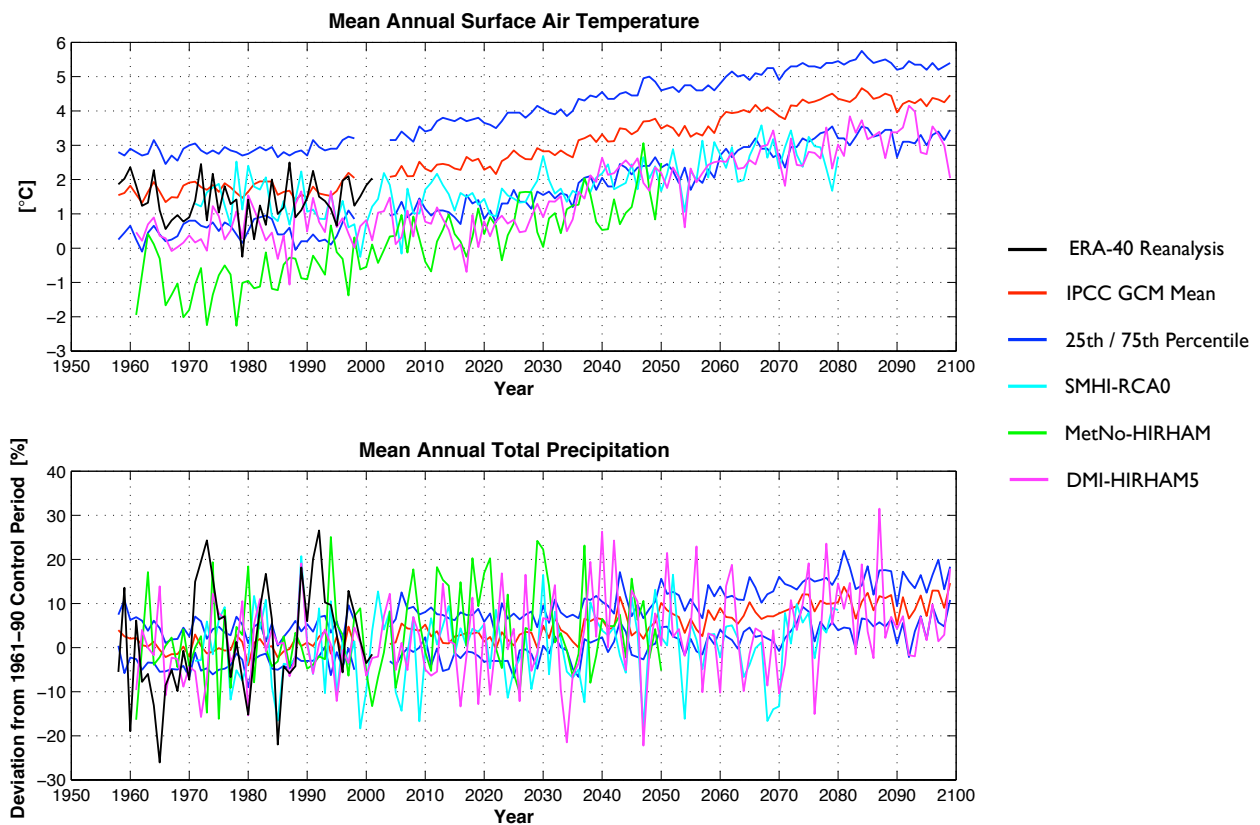
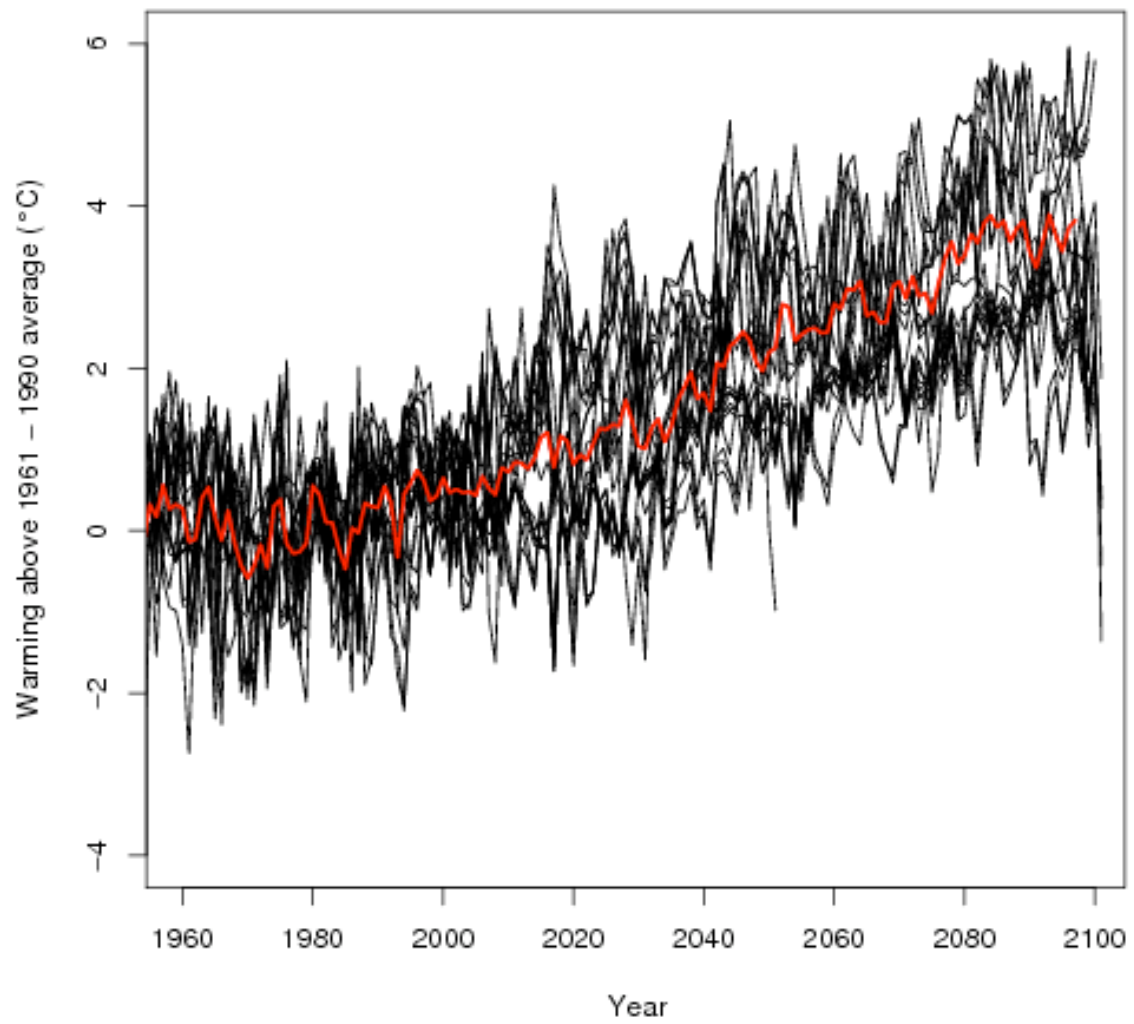


Figure 14. Mean annual values of surface air temperature and total precipitation, averaged over the land area of Iceland, for the reanalyses, the GCM ensemble mean, and the RCMs. The blue lines indicate the 25th and 75th percentile of the GCM ensemble spread based on a normal distribution.



*Figure 15. Mean annual values of surface air temperature over Iceland based on 24 RCMs included in the ENSEMBLES project.*

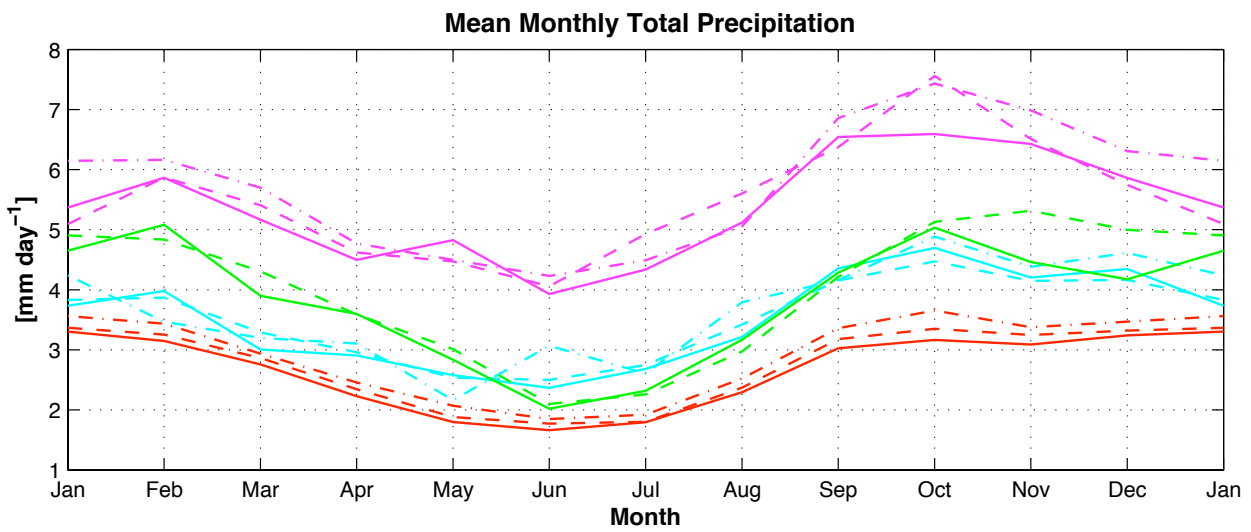
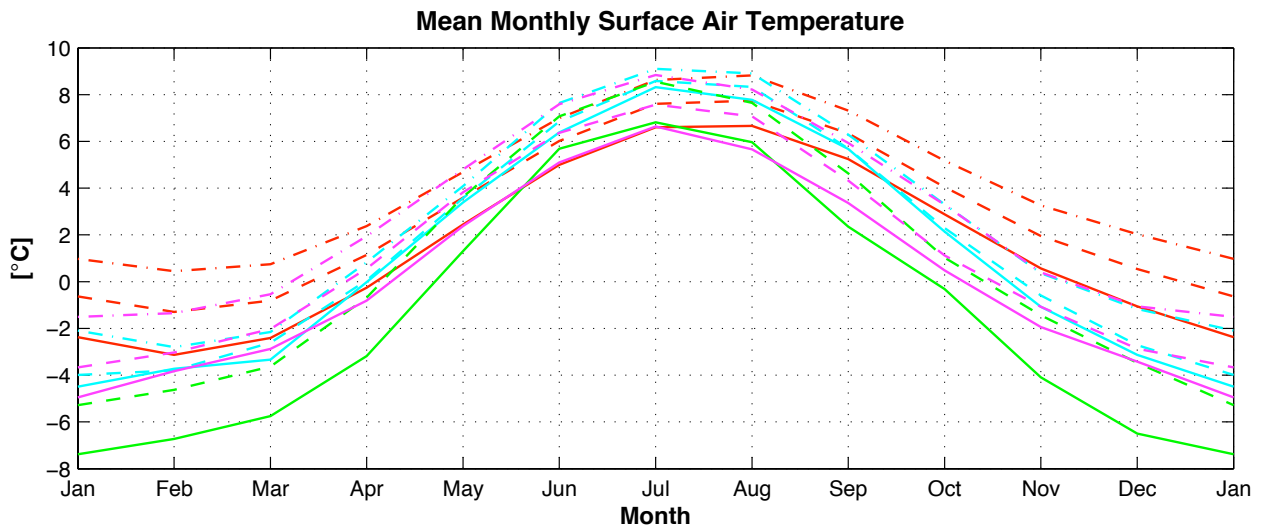


Figure 16. Mean seasonal cycle during the 1961–90 control period (solid lines), the 2021–50 reference period (dashed lines), and the 2070–99 reference period (dash-dotted lines), for the IPCC ensemble mean (red lines), the SMHI-RCAO (cyan lines), the MetNo-HIRHAM (green lines), and the DMI-HIRHAM5 (magenta lines).

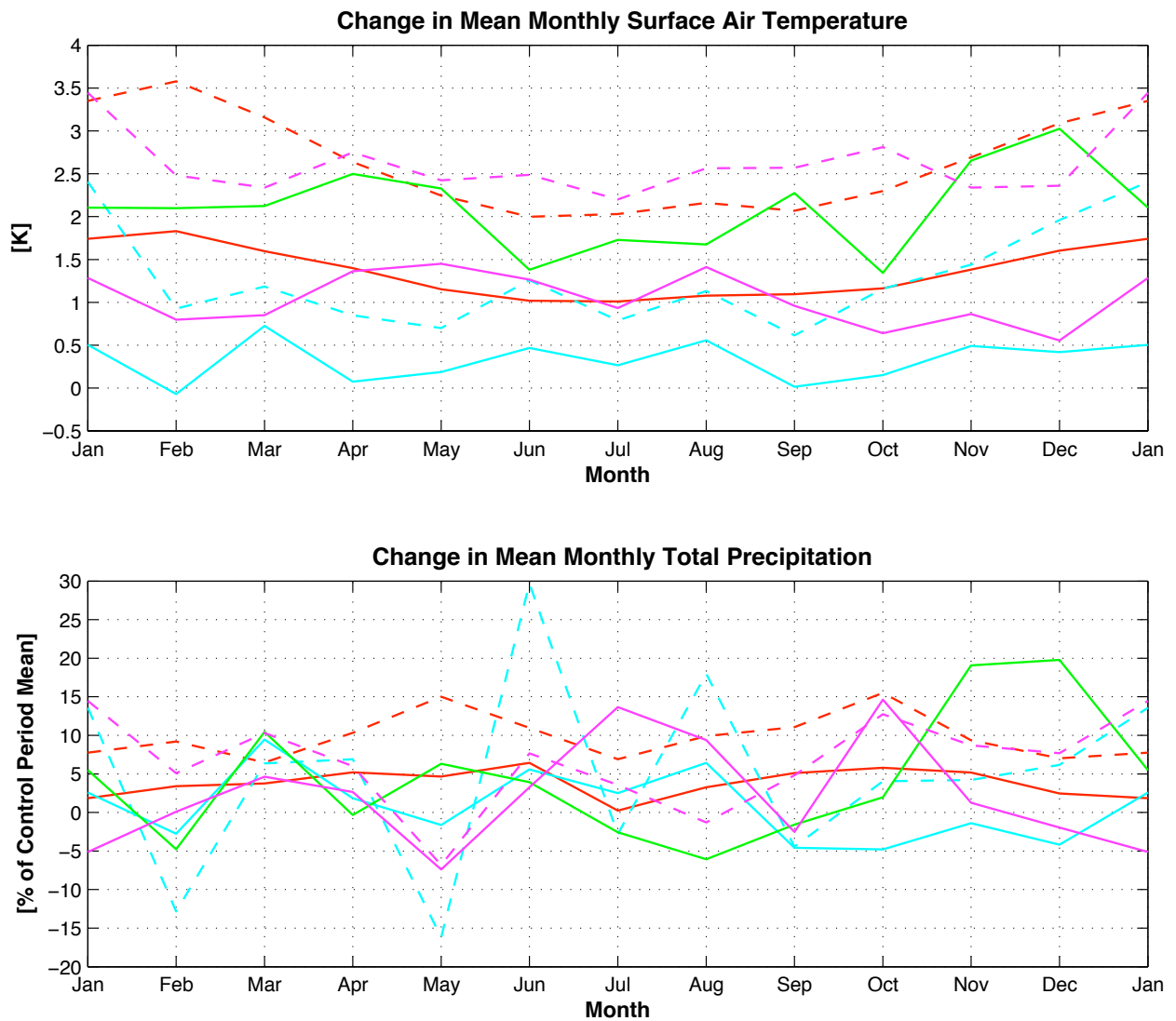


Figure 17. Changes in the mean seasonal cycle from the 1961–90 control to the 2021–50 reference period (solid lines), as well as changes from the control to the 2070–99 reference period (dashed lines), for the reduced IPCC ensemble mean (red lines), the SMHI-RCAO (cyan lines), the MetNo-HIRHAM (green lines), and the DMI-HIRHAM5 (magenta lines).

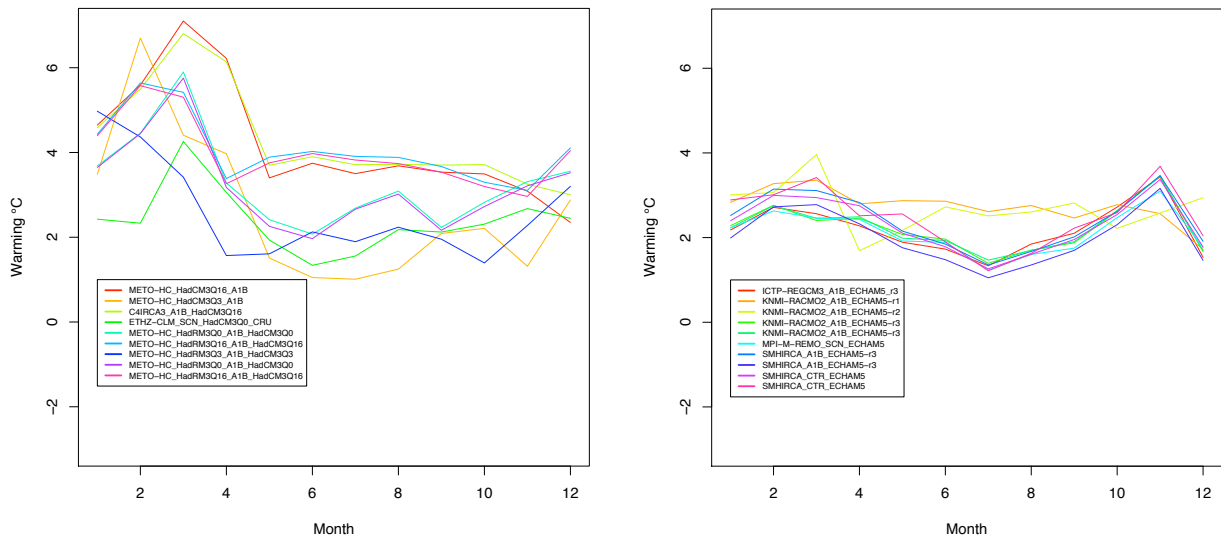


Figure 18. Warming by month from the 1991–2000 to the 2091–2100 period in ENSEMBLES RCMs using either the HadCM3 (left) or the ECHAM5 (right) as driving GCM.



## References

- Bergþórsson, P., Björnsson, H., Dýrmundsson, Ó., Guðmundsson, B., Helgadóttir, A., and Jónmundsson, J. V. (1987). The effect of climatic variations on agriculture (*in Icelandic*). In Parry, M. L., Carter, T. R., and Konijn, N. T., editors, *The impact of climatic variations on agriculture*, volume 1 of *Assessments In Cool Temperate and Cold Regions*, pages 381–509, Dordrecht, The Netherlands. Reidel.
- Björnsson, H., Jónsson, T., Gylfadóttir, S. S., and Ólason, E. Ó. (2007). Mapping the annual cycle of temperature in Iceland. *Meteorol. Z.*, 16(1):45–56.
- Crochet, P., Jóhannesson, T., Jónsson, T., Sigurðsson, O., Björnsson, H., Pálsson, F., and Barstad, I. (2007). Estimating the spatial distribution of precipitation in Iceland using a linear model of orographic precipitation. *J. of Hydrometeorol.*, 8(6):1285–1306.
- Engen-Skaugen, T. (2007). Refinement of dynamically downscaled precipitation and temperature scenarios. *Climatic Change*, 84:365–382.
- Fenger, J. (2007). *Impacts of climate change on renewable energy sources: Their role in the Nordic energy system*. Nordic Council of Ministers, Copenhagen, Denmark.
- Hansen, J., Lacis, A., Rind, D., Russel, G., Stone, P., Fung, I., Ruedy, R., and Lerner, J. (1984). Climate sensitivity: Analysis of feedback mechanisms. In Hansen, J. E. and Takahashi, T., editors, *Climate Processes and Climate Sensitivity*, volume 29 of *AGU Geophysical Monograph*, pages 130–163, Boston, Massachusetts, USA. American Geophysical Union.
- Hansen, J., Russel, G., Rind, D., Stone, P., Lacis, A., Lebedeff, S., Ruedy, R., and Travis, L. (1983). Efficient three-dimensional global models for climatic studies: Models I and II. *Mon. Wea. Rev.*, 111(4):609–662.
- Haugen, J. E. and Iversen, T. (2006). Response in daily precipitation and winds speed extremes from HIRHAM downscaling of SRES B2 scenarios. RegClim General Technical Report 8, Norwegian Meteorological Institute, P.O. Box 43 Blindern, NO-0313 Oslo, Norway.
- IPCC (2001). *Climate Change 2001: The Scientific Basis*. Cambridge University Press for the Intergovernmental Panel on Climate Change, Cambridge, England.
- IPCC (2007). *Climate Change 2007: The Physical Science Basis*. Cambridge University Press for the Intergovernmental Panel on Climate Change, Cambridge, England.
- Jóhannesson, T., Aðalgeirsdóttir, G., Björnsson, H., Crochet, P., Elíasson, E. B., Guðmundsson, S., et al. (2007). Effect of climate change on hydrology and hydro-resources in Iceland. Report OS-2007/011, National Energy Authority, Reykjavik, Iceland.
- Jóhannesson, T., Jónsson, T., Källén, E., and Kaas, E. (1995). Climate Change Scenarios for the Nordic Countries. *Climate Research*, 5:181–195.
- Jónasson, K. (2004). Spá um meðalhita í Reykjavík á 21. öld. *Tímarit um Raunvísindi og Stærðfræði*, 2:25–40.

- Kaas, E. (1993). Greenhouse induced climate change in the Nordic countries as simulated with the Hamburg climate model. Part 2: Statistical interpretation. Scientific Report 93-3, Danish Meteorological Institute, Copenhagen.
- Kaas, E. (1994). An update of statistically interpreted greenhouse induced climate change in the Nordic countries. Informal Report, Danish Meteorological Institute, Copenhagen.
- Kjellstöm, E. (2009). Deliverables 4.3: Report on user dialogue and analysis of regional climate scenarios for northern Europe. Draft Report, pp. 160, Swedish Meteorological and Hydrological Institute, Folkborgsvägen 1, 601 76 Norrköping, Sweden.
- Koenigk, T., Döscher, R., and Nikulin, G. (2011). Arctic future scenario experiments with a coupled regional climate model. *Tellus A*, 63:69–86.
- Ministry for the Environment (2000). Veðurfarsbreytingar og afleiðingar þeirra. Skýrsla vísindanefndar um loftslagsbreytingar, Government of Iceland, Reykjavík.
- Ministry for the Environment (2008). Hnattrænar loftslagsbreytingar og áhrif þeirra á Íslandi. Skýrsla vísindanefndar um loftslagsbreytingar, Government of Iceland, Reykjavík.
- Uppala, S. M., Kållberg, P. W., Simmons, A. J., et al. (2005). The ERA-40 re-analysis. *Q. J. R. Meteorol. Soc.*, 131:2961–3012.
- van der Linden, P. and Mitchell, J. F. B. (2009). ENSEMBLES: Climate change and its impacts. Summary of research and results. Final Report, 19 pp., Met Office Hadley Centre, FitzRoy Road, Exeter EX1 3PB, UK.